

# Lawrence Berkeley National Laboratory

## Recent Work

### Title

The Aluminum-Scandium-Lithium-Magnesium System as a Potential Source of Superplastically Formable Alloys

### Permalink

<https://escholarship.org/uc/item/0m45d7xc>

### Author

Emigh, R.A.

### Publication Date

1990-07-01

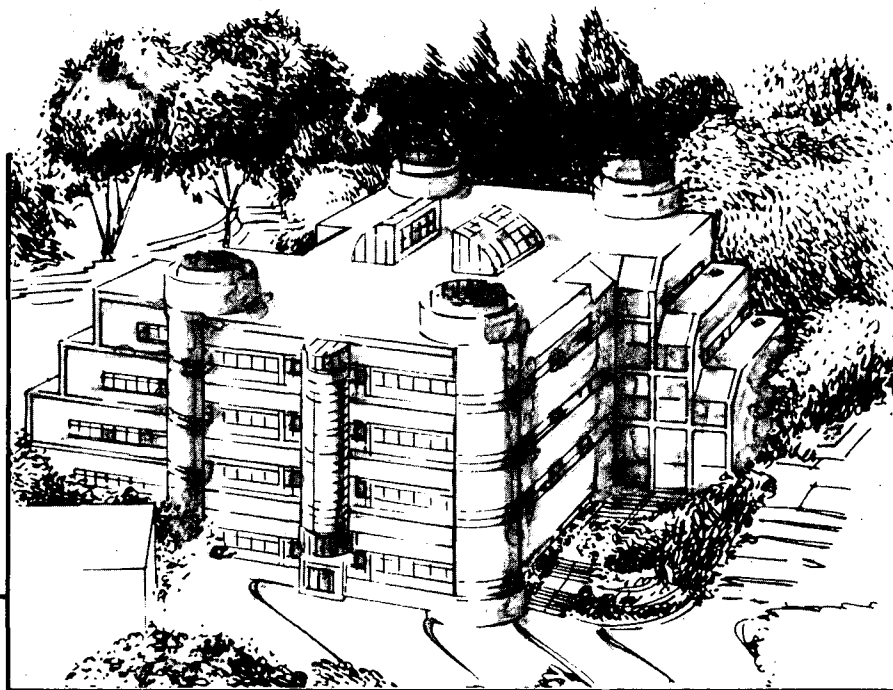
Center for Advanced Materials

# CAM

## The Aluminum-Scandium-Lithium-Magnesium System as a Potential Source of Superplastically Formable Alloys

R.A. Emigh  
(Ph.D. Thesis)

July 1990



**Materials and Chemical Sciences Division**  
**Lawrence Berkeley Laboratory • University of California**  
 ONE CYCLOTRON ROAD, BERKELEY, CA 94720 • (415) 486-4755

Prepared for the U.S. Department of Energy under Contract DE-AC03-76SF00098

1 LOAN COPY 1  
 1 Circulates 1  
 1 for 2 weeks 1

Bldg. 50 Library.  
 Copy 2

LBL-29355

## **DISCLAIMER**

This document was prepared as an account of work sponsored by the United States Government. While this document is believed to contain correct information, neither the United States Government nor any agency thereof, nor the Regents of the University of California, nor any of their employees, makes any warranty, express or implied, or assumes any legal responsibility for the accuracy, completeness, or usefulness of any information, apparatus, product, or process disclosed, or represents that its use would not infringe privately owned rights. Reference herein to any specific commercial product, process, or service by its trade name, trademark, manufacturer, or otherwise, does not necessarily constitute or imply its endorsement, recommendation, or favoring by the United States Government or any agency thereof, or the Regents of the University of California. The views and opinions of authors expressed herein do not necessarily state or reflect those of the United States Government or any agency thereof or the Regents of the University of California.

**The Aluminum-Scandium-Lithium-Magnesium System as a  
Potential Source of Superplastically Formable Alloys**

Roger Alan Emigh

Pd.D. Dissertation

Department of Materials Science and Mineral Engineering  
University of California

and

Center for Advanced Materials  
Materials and Chemical Sciences Division  
Lawrence Berkeley Laboratory  
1 Cyclotron Road  
Berkeley, CA 94720

July 1990

This work was supported by the Director, Office of Energy Research, Office of Basic Energy Science, Materials Sciences Division of the U. S. Department of Energy under Contract No. *DE-AC03-76SF00098*. The Aluminum Company of American contributed the Al-Sc master alloy used in this research

# The Aluminum-Scandium-Lithium-Magnesium System as a Potential Source of Superplastically Formable Alloys.

by

Roger Alan Emigh

## ABSTRACT

Alloys from the aluminum-lithium-scandium-magnesium system have been cast and rolled for study. The goal is to evaluate this system for the development of superplastically formable, high strength alloys. Aluminum-scandium-magnesium alloys have shown potential as superplastic alloys. These alloys rely on small  $\text{Al}_3\text{Sc}$  (ordered  $\text{L}_{12}$ ) precipitates for grain structure stabilization and strengthening. Additional precipitation strengthening is required to raise their strength to levels sufficient for aircraft applications. The addition of lithium provides this additional strengthening through the formation of  $\text{Al}_3\text{Li}$  ( $\delta'$ ).

To produce the alloys studied in this research, a unique induction melting furnace was constructed that incorporates special features to produce aluminum-lithium alloys with low hydrogen content. The furnace also features a water cooled, copper casting mold to achieve a moderately rapid solidification rate. This is because the amount of scandium used (0.5 wt. %) is in excess of the solubility limit and  $\text{Al}_3\text{Sc}$  cannot be re-solutionized to any extent. It is therefore desired to super-saturate the matrix with as much scandium as possible for later precipitation.

Two high lithium alloys were produced, ALS2 (nominal composition Al-2.2Li-0.5Sc) and ALS4 (nominal composition Al-2.0Li-2.2Mg-0.5Sc) that were strengthened with  $\delta'$  ( $\text{Al}_3\text{Li}$ ). These alloys exhibited strength and ductility superior to those of aluminum-lithium-(magnesium)-zirconium alloys. This is because the scandium containing alloys have developed a finer grain structure and the  $\text{Al}_3\text{Sc}$  precipitates contribute to the alloys strength.

## Table of Contents

1.	Introduction .....	1
2.	Microstructural Background .....	4
	2.1. Aluminum-Scandium-Magnesium Alloys .....	4
	2.2. Aluminum-Lithium Alloys .....	5
	2.3. Aluminum-Lithium-Scandium Alloys .....	7
	2.4. Aluminum-Lithium-Magnesium Alloys .....	7
3.	Material Production .....	9
	3.1. Light Alloy Melting Facility .....	9
	3.2. Special Casting Requirements .....	9
	3.2.1. Hydrogen .....	9
	3.2.2. Oxygen .....	11
	3.2.3. Solution: Hydrogen and Oxygen .....	11
	3.2.2. Alkali Metal Impurities .....	12
	3.2.3. Solidification Rate .....	13
	3.3. Melting Procedure .....	14
	3.3.1. Carbon Filter .....	14
	3.3.2. Crucible Design .....	14
	3.3.3. Furnace Assembly .....	15
	3.3.4. Charge Preparation .....	16
	3.3.5. Melting/Casting .....	16
	3.4. Alloys Produced .....	18
4.	Experimental Procedure .....	19
	4.1. Thermomechanical Processing .....	19
	4.1.1. Low Lithium Alloys .....	19
	4.1.2. High Lithium Alloys .....	19
	4.1.3. High Lithium Alloys with Magnesium .....	21
	4.2. Mechanical Testing .....	21
	4.3. Slip Line Traces .....	24
	4.4. Fracture Surfaces .....	24
5.	Discussion .....	25
	5.1. Microstructure Characterization .....	25
	5.1.1. As-Cast Material .....	25
	5.1.2. Rolled Sheet .....	25

5.1.2.1. Melting Study .....	26
5.1.2.2. Phase Equilibrium Study .....	27
5.1.3. Aging .....	29
5.2. Mechanical Properties .....	29
5.2.1. Aluminum-Scandium .....	30
5.2.2. Aluminum-Scandium-Lithium .....	30
5.2.3. Aluminum-Scandium-Lithium-Magnesium .....	31
5.3. Slip Line Tracings .....	32
5.4. Effect of Deformation on $\nu$ phase .....	33
5.5. Tensile Fracture Surfaces .....	34
6. Summary and Conclusions .....	35
6.1 Early Superplastic Data .....	35
7. Recommendations For Future Work .....	36
8. Acknowledgments .....	37
9. References .....	38
Appendix 1. Quantitative Auger Analysis .....	41
Figure Captions .....	43
Figures .....	45

## 1. INTRODUCTION

In future generations of aircraft and space vehicles, there will be increasing competition between advanced structural materials. Designers of these weight critical structures are continually looking for lighter, stronger, stiffer, and less expensive materials. Great effort is currently being expended to improve the competitiveness of aerospace aluminum alloys. Much of this research is on aluminum-lithium alloys because they offer a density reduction and stiffness increase over commercial aluminum alloys. Another area of increasing research is into the development of superplastically formable aluminum alloys.

One significant advantage that aluminum alloys currently hold over engineered materials, such as polymer and metal matrix composites, is a relatively low manufacturing cost. Through the use of superplastic forming it is possible to improve on this advantage by allowing the manufacturer to produce complex, near net-shape parts. This lowers production costs by reducing or eliminating the need for fasteners, expensive dies, and machining. There is also a reduction in the amount of waste material generated largely due to the decreased amount of machining required. The cost factor of this waste material becomes increasingly important as the cost of the alloy increases.

Currently, the best high strength aluminum alloy that can be superplastically formed is 7475 (nominal composition Al-6.0Zn-2.0Mg-2.0Cu)<sup>1,2</sup>. [NOTE: Throughout this thesis all elemental compositions are given in weight percent] It has a density of 2.82 g/cm<sup>3</sup>, elastic modulus is 70.0 GPa, and T6 (solution heat treated and peak aged) mechanical properties of 490 MPa (71 ksi) yield, 550 MPa (80 ksi) ultimate with 12% elongation. The principal drawbacks to this alloy are that it is superplastic only at low strain rates ( $10^{-4}$  / seconds) and its density is too high. An aluminum alloy with similar mechanical properties, higher superplastic strain rates, and lower density would be of great use to the aerospace industry.



Recently, work by Sawtell at Alcoa discovered that Al-Sc-Mg alloys have unique superplastic properties<sup>3</sup>. Al-4.0Mg-0.5Sc alloy exhibited elongations of >1000% at 400°C for a strain rate of  $10^{-2}$ /s. The exceptional superplastic behavior of this alloy is attributed to the presence of very fine Al<sub>3</sub>Sc precipitates. These ordered precipitates stabilize the grain structure by inhibiting recrystallization and cause Al-Sc alloys to develop fine subgrains during rolling. With the addition of magnesium, the subgrain size decreases and this leads to the exceptional superplastic properties seen in the Al-4.0Mg-0.5Sc alloy.

The Al<sub>3</sub>Sc phase is a very potent strengthener because it can be formed as very small precipitates and these are thermally stable to 300°C. The solubility limit of scandium in aluminum is only 0.38% at 660°C and drops rapidly with decreasing temperature. Using mildly rapid solidification it is possible to get 0.52% (the eutectic composition) into solution. Even at this low solute level, the Al<sub>3</sub>Sc precipitates are able to significantly increase strength because they are looped by dislocations at diameters of only 7 nm<sup>4</sup>. This means that maximum strength will occur with a distribution of very small precipitates.

In Alcoa's work, relatively high strengths were achieved by extensively warm rolling (288°C) and cold rolling the magnesium containing alloys. Magnesium is a very effective solid solution strengthener of aluminum base alloys due to its large misfit with the aluminum lattice<sup>5</sup>. Also, alloys containing magnesium can be substantially strengthened by cold working. This is due to magnesium's ability to lower the stacking fault energy of aluminum which reduces the amount of dislocation annihilation that occurs; the alloys tend to develop a network of fine subgrains and retain a higher dislocation density than magnesium free alloys. However, superplastic forming significantly changes this microstructure.

Superplastic deformation in these alloys is observed to occur between 400°C and 500°C. This temperature is high enough to destroy the effect of the cold work and to

severely overage the  $\text{Al}_3\text{Sc}$  precipitates in a very short period of time. Obviously, it is impossible to impart cold work on a superplastically formed part. The result is that superplastically formed material from the Al-Sc-Mg system has very low strength with no post-forming method (cold rolling or precipitation strengthening) of increasing it. The addition of a quaternary alloying element (X) is therefore required that will give Al-Sc-Mg-X alloys the ability to be age hardened after forming.

The requirements for this quaternary alloying element are that it be completely solutionized at the superplastic forming temperature and then allow precipitation hardening after forming. A brief inspection of other precipitation hardened aluminum-alloys reveal several candidate elements: copper, lithium, zinc, or silicon. In keeping with the quest for low density, lithium becomes the choice for the quaternary addition in this research.

Lithium is the only element (besides Beryllium, which is generally avoided for health and safety reasons) that simultaneously lowers density and increases stiffness of aluminum-base alloys. The addition of each weight percent of lithium reduces the density of aluminum alloys by  $\approx 3\%$  and increases their stiffness by  $\approx 5\%$ <sup>6</sup>. It also acts as a potent precipitation strengthener through the formation of  $\delta'$ , an ordered  $\text{L}_{12}$  phase with stoichiometric composition  $\text{Al}_3\text{Li}$ . These advantages do not come without some drawbacks. The production of lithium containing alloys is significantly more difficult and these problems will be fully discussed in the Material Production section of this thesis.

The overall purpose of this research is to lay the foundation for the development of high strength, low density Al-Sc-Li-Mg alloys. These alloys are targeted to be superplastically formable with the ability to be aged to high strength after forming. The specific goals were: develop a method for producing these alloys, study the microstructure developed during and after thermomechanical processing of the ingots, and to mechanically test the unformed material after aging. The superplastic testing and study of its effects on these alloys will be performed in a subsequent research project<sup>7</sup>.

## 2. Microstructural Background

When performing an alloy development project, it is critical to understand the effect that each possible alloying element will have on the alloy system. The starting point of any such project should be the accumulation of the existing information on the alloy systems of interest. For instance, the Al-Mg and Al-Li systems are well understood and a large amount of data exists for them. The available data includes phase diagrams, thermomechanical processing information, heat treatment practice and characterization of the microstructures observed. There is less information available for the Al-Sc, Al-Sc-Mg and Al-Li-Mg systems. There is no useful information available on the Al-Sc-Li.

It was determined that the best research method was to start with the Al-Sc system and add lithium to it. The precipitation reactions that occur in this system are of particular interest because the phases that form ( $\text{Al}_3\text{Li}$  and  $\text{Al}_3\text{Sc}$ ) are isomorphic. Once a basic knowledge of this system was established, magnesium was added and the quaternary system was studied.

### 2.1. Aluminum-Scandium-Magnesium Alloys

Scandium is the most potent strengthening element on a per atom basis available for use in aluminum-base alloys<sup>8,9,10</sup>. The source of this behavior is the presence of very fine  $\text{Al}_3\text{Sc}$  precipitates that exist in an ordered  $\text{L}_{12}$  structure. These precipitates are also very effective at stabilizing the grain structure by preventing grain boundary motion. This allows aluminum-base alloys containing scandium to be processed into a superplastic microstructure consisting of a small, thermally stable grain size<sup>11</sup>. The Al-Sc phase diagram (Figure 2.1) shows that only about 0.52% scandium can be added without the formation of primary  $\text{Al}_3\text{Sc}$  during casting and once the  $\text{Al}_3\text{Sc}$  forms, it cannot be resolutionized. This limits the amount of strengthening achievable. Even at this low solute level, yield strengths up to 275 MPa (40 ksi) have been achieved for optimally processed

Al-0.5Sc binary alloys. However, it should be noted that during the processing and aging of these alloys, temperatures were kept below 300°C to prevent irreversible overaging of the strengthening precipitates. Since superplastic behavior of aluminum-base alloys is normally observed at above 400°C, overaging of the Al<sub>3</sub>Sc is inevitable with a corresponding loss of strength.

## 2.2. Aluminum-Lithium Alloys

The aluminum rich end of the Al-Li system (Figure 2.2<sup>12</sup>) is characterized by a eutectic invariant at 602°C between  $\alpha$ -aluminum and AlLi ( $\delta$ ). Delta is very important to the alloy designer because of its notorious ability to degrade the properties of Al-Li alloys. It is a congruent melting phase that decomposes to liquid at 717°C and has crystal structure that is cubic (B<sub>32</sub>) with a lattice parameter of 0.637nm<sup>13</sup>. It forms heterogeneously at grain boundaries. As it grows, the  $\delta$  absorbs lithium from the grain boundary area. This causes a  $\delta'$  precipitate free zone (PFZ) to form in the vicinity of the  $\delta$  precipitate. Since the PFZ is weaker than the grain interiors, strain will localize there, leading to intergranular failure of the material.

The other aluminum-rich intermetallic is the metastable, ordered phase Al<sub>3</sub>Li ( $\delta'$ ). This is the strengthening phase of this system and can form homogeneously by a spinodal decomposition<sup>14</sup> or heterogeneously on dispersoids<sup>15</sup>. The spinodal type of transformation can occur after quenching from high temperature if enough lithium is kept in solid solution. This decomposition occurs by the following sequence: the super saturated  $\alpha$ -solution orders congruently, this structure decomposes spinodally into high-lithium regions (Al<sub>3</sub>Li) and low-lithium regions, and finally, the low lithium regions disorder into  $\alpha_{SS}$ . A significant benefit of this type of phase transformation is that it occurs without a nucleation barrier so  $\delta'$  is formed uniformly throughout the matrix.

The  $\delta'$  has a very low mismatch with the aluminum lattice, allowing complete coherency at all precipitate sizes. Precipitates of  $\delta'$  resist shear because an antiphase

boundary is formed when a unit dislocation passes through them. This antiphase boundary is eliminated when another unit dislocation passes through the precipitate and because of this, the dislocations are commonly observed to travel in pairs called superdislocations<sup>16,17,18</sup>. Unfortunately, with each successive dislocation pair, the sheared plane decreases in area with an accompanying decrease in antiphase boundary energy that reduces the precipitates resistance to further shear. As deformation continues there is a localization of strain that produces stress concentrations at dislocation blocks (ie grain boundaries, non-shearable dispersoids). Al-Li binary alloys are notorious for exhibiting low ductility and this is generally attributed to these stress concentrations at grain boundaries caused by the localized deformation. One method of reducing these stress concentrations is to reduce the grain size.

In order to control the grain structure of Al-Li alloys, most contain zirconium additions of 0.1% to 0.2%. This causes  $\beta'$  ( $\text{Al}_3\text{Zr}$ ) to form, which slows grain growth and inhibits recrystallization by blocking grain boundaries in the same manner as  $\text{Al}_3\text{Sc}$  does. This allows Al-Li-Zr alloys to be processed into an elongated, unrecrystallized grain structure that improves the strength and ductility of these alloys.

To further improve the strength, ductility, and toughness of  $\text{Al}_3\text{Li}$  strengthened alloys, the current generation of commercial Al-Li-Zr alloys employ an additional alloying element that incorporates lithium into another strengthening phase. The most successful of these alloys use a 2-3% copper addition. The high strength developed by these alloys is dependent on the homogeneous precipitation of the plate-like phase  $T_1$  ( $\text{Al}_2\text{CuLi}$ ). Unfortunately, this phase has a high nucleation barrier and will normally form at grain boundaries. To obtain a homogeneous distribution of the  $T_1$  phase, these alloys are commonly stretched (6-8%) prior to aging. This stretching produces a uniform distribution of dislocations that act as nucleation sites for  $T_1$ . However, this requirement places some serious restrictions on ability of these alloys to be used in superplastically formed parts. As a result, recent attempts to use conventional Al-Li-Cu-Zr alloys for

superplastic applications have been unsuccessful due to an inability to generate sufficient strength in the superplastically formed material<sup>19,20</sup>. To produce a high strength, superplastic Al-Li alloy it will be necessary to eliminate the copper and its accompanying precipitates. Because copper increases the density of aluminum alloys, its removal also provides a welcome reduction in alloy density.

### 2.3. Aluminum-Lithium-Scandium Alloys

While the Al-Li system has been extensively studied since 1950 and the Al-Sc system has been explored in recent years by several researchers, the Al-Li-Sc system has only been briefly studied by Gayle<sup>21</sup>, with little success. In that research, scandium was selected in an attempt to modify the lattice misfit of  $\delta'$  ( $\text{Al}_3\text{Li}$ ). They produced a single ingot of Al-2.8Li-2.0Sc-1.1Fe that weighed about 250 grams. This ingot was homogenized for 24 hours at 500°C, extruded 10:1 at 400°C, then solution heat treated for 0.5 hour at 525°C before aging for 4 hours at 190°C. The mechanical properties for this alloy and treatment were: 400MPa (58ksi) yield, 420MPa (61ksi) ultimate, and 2% elongation.

Although this alloy achieved relatively high strength, it proved to have almost no ductility. Problems with the melting practice introduced large quantities of Fe impurities into the alloys. Because of this, the alloy contained large quantities of interdendritic, insoluble iron particles. The amount of scandium (2.0%) was far in excess of the solubility limit (0.5%) and this was compounded by homogenizing the ingot at high temperature. This overaged the scandium precipitates to even larger sizes that were certainly detrimental to the alloy ductility.

### 2.4. Aluminum-Lithium-Magnesium Alloys

Magnesium is a very good solid solution strengthener of aluminum-base alloys due primarily to its relatively large misfit with the aluminum lattice<sup>22</sup>. In alloys containing

scandium it also improves the superplastic behavior by refining the microstructure<sup>23</sup>. The subgrain size developed in Al-Sc-Mg is seen to decrease with increasing magnesium content and this correlates to improved superplastic behavior.

In Al-Li alloys, the addition of magnesium reduces the solubility of lithium in the matrix and increases the amount of  $\text{Al}_3\text{Li}$  that forms. However, there is also a ternary phase, S ( $\text{Al}_2\text{LiMg}$ ), that can form in alloys containing sufficient quantities of magnesium ( $\approx 2.0\%$ ) and lithium ( $\approx 1.0\%$ )<sup>24,25</sup>.

### 3. MATERIAL PRODUCTION

#### 3.1. Light Alloy Melting Facility

In order to produce the alloys studied for this research, a highly specialized melting facility was needed. Such a facility (Figure 3.1) has been designed and constructed by the author at the Lawrence Berkeley Laboratory. Designated the Light Alloy Melting Facility (LAMF), it is a vacuum induction melting furnace that has proved very successful at producing quality ingots of Al-Li alloys.

The most important items to be addressed when casting Al-Li alloys are: hydrogen content of the melt, oxide formation, and alkali metal impurities. When producing scandium containing alloys it is also desirable to produce a moderately rapid solidification rate for previously discussed reasons. Several special features are designed into this furnace specifically to cope with all of these problems, especially the reactivity and affinity for water of the lithium-containing molten alloys.

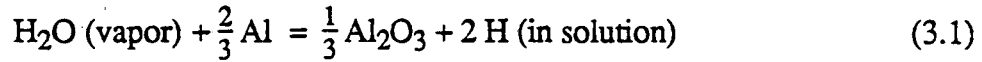
#### 3.2. Special Casting Requirements

##### 3.2.1. Hydrogen

The single most important thing when producing Al-Li alloys is to limit the amount of hydrogen in the melt. Hydrogen has a relatively high solubility in molten aluminum (1 ppm) but has a very low solubility (0.05 ppm) in the solidified metal. If the hydrogen content at casting is above 0.05 ppm, it will be rejected during solidification into the remaining liquid. This enriches the remaining molten metal and when the solubility limit is exceeded, hydrogen bubbles will form, causing micro-porosity in the ingot. If this casting porosity occurs it severely degrades the ingot properties.

The reason that hydrogen presents such a problem with Al-Li alloys lies with the lithium alloying addition. Lithium has a strong affinity for water and carries some moisture into the melt. Water dissociates in molten aluminum by the equation:





Water can also come from other sources: the crucible, furnace atmosphere, and from the other alloying elements. Efforts to minimize the amount of hydrogen from these sources are beneficial but there will always be some excess hydrogen that must be removed.

It is possible to remove the dissolved hydrogen by flushing the melt with an inert gas<sup>26</sup>. The basis for this is the existence of a difference in hydrogen activity in the melt and inert gas bubbles. This thermodynamic removal of hydrogen depends on the equation:

$$\frac{1}{[\text{H}_{\text{ppm}}]_t} - \frac{1}{[\text{H}_{\text{ppm}}]_i} = \frac{k_h V t}{W} \quad (3.2)$$

which relates the reduction in hydrogen from an initial value,  $[\text{H}_{\text{ppm}}]_i$  to a lower value at after flushing,  $[\text{H}_{\text{ppm}}]_t$ . Other variables are the inert gas flow rate ( $V$ ), time of flushing ( $t$ ), and weight of the melt ( $W$ ).  $k_h$  is a constant that relates the transfer of hydrogen from the melt to the flush gas. This equation gives the minimum volume of flushing gas that is required to reduce the level of hydrogen to the desired level. In real systems there are always kinetic factors that reduce the efficiency of this degassing.

In order for hydrogen to be removed, it must contact the surface of an inert gas bubble and then diffuse across the liquid-gas interface. For complete diffusional control the governing equation is:

$$\ln \frac{\text{H}\%}{\text{H}\%_i} = - \frac{k_{\text{mH}} \rho^A}{W} t \quad (3.3)$$

where  $k_{\text{mH}}$  is the mass transfer coefficient for hydrogen,  $\rho$  and  $W$  are the density and weight of the melt,  $A$  is the total surface area of the flushing gas in contact with the molten metal, and  $t$  is the total flushing time. Fixing  $W$  and  $t$ , the maximum hydrogen removal

rate is obtained by maximizing the term  $[k_{mH} \rho^A]$ . Both  $k_{mH}$  and  $A$  increase as the size of the gas bubbles decrease. Maximum removal is therefore favored by small bubbles because they present the most surface area per volume of flushing gas.

It is now possible to summarize the capabilities of inert gas flushing of aluminum-alloy melts to remove hydrogen. As the hydrogen content drops, it becomes increasingly difficult to remove. Additionally, the amount of hydrogen removed depends not only on the volume of flushing gas but also on the diffusionally controlled efficiency. This degassing efficiency is dependent on the size of the gas bubbles and the amount of molten metal that they come into contact with.

### 3.2.2. Oxygen

Aluminum alloys always form an oxide dross when they are melted. The oxygen for this reaction can come from any of several sources: aluminum oxide on the charge surface, oxygen from ceramic crucibles, or from the furnace atmosphere. When alloying with lithium, oxide formation becomes even more of a problem because lithium is also a strong oxide former. These oxides are undesirable in the cast material because they act as insoluble inclusions that are detrimental to ductility and toughness. The presence of insoluble oxides has been a major problem in the attempt to develop Al-Li powder metallurgy alloys using rapid solidification<sup>27</sup>.

### 3.2.3. Solution: Hydrogen and Oxygen

To combat the problems with oxygen and hydrogen, the entire melting facility is situated in a containment vessel which allows melting to be carried out in a dry argon atmosphere that has been thoroughly flushed of impurity gases and water. This effectively limits the amount of hydrogen and oxygen from the dissociation of water vapor that can enter the melt from the furnace atmosphere. However, considerable hydrogen is still introduced into the melt with the lithium alloying addition and the hydrogen concentration must be reduced prior to casting.

To allow inert gas flushing, the furnace has a vertical design with the crucible/induction coil positioned directly above the casting chill mold (Figure 3.1). Between these two regions is a porous graphite filter and a transition plenum connected to a vacuum system. By supporting the melt with a porous filter, an increase in the argon pressure in the area below the filter (plenum) causes argon to pass up through the melt. The efficiency of this degassing is dependent on producing small argon bubbles and passing them through the maximum amount of metal. Due to the induction field, the top of the melt rises into a dome (Figure 3.2) and this creates a short cut for the argon to pass up the side of the crucible. When this happens, the argon is in contact with the crucible wall and the melt, thus reducing the surface area of flush gas available for hydrogen removal. Also, the metal tends to splash up the side of the crucible and out of the top of the furnace, forcing the flow of argon to be reduced. To counter this, the filter is machined to be thinner in the center, thus causing the argon to pass through more of the melt and this improves the degassing efficiency.

This type of a melting setup also is beneficial with respect to oxide dross formation. The density of  $\text{Al}_2\text{O}_3$  is very close to that of molten aluminum and does not rise to the surface. The bubbling inert gas tends to push this dross material towards the top of the melt. Then the metal must pass through the carbon filter during casting. These two effects combine to eliminate the majority of oxide inclusions from the ingots. In practice, it was found that the used filter always had a moderate amount of dross remaining on it after casting. Another beneficial side effect of this degassing is improved mixing of the melt, which quickly distributes the elemental lithium added to the melt.

### 3.2.3. Alkali Metal Impurities

Unlike lithium, other alkali metals (sodium, potassium) have very low solubilities in aluminum. It has been documented in Al-Li alloys that sodium levels above 500 ppm cause dramatic reductions in ductility and toughness<sup>28,29</sup>. Examination of the periodic table reveals that sodium and lithium belong to the same period and as such sodium is a

rather common impurity element in lithium. The solution to this alloying problem is relatively simple: use only lithium with low sodium content. The alloy grade lithium that was used for this research contained <100 ppm of sodium. For a 2% lithium ingot this yields a sodium concentration of 10 ppm, much lower than has been identified as causing problems in Al-Li alloys.

#### 3.2.4. Solidification Rate

Once the  $\text{Al}_3\text{Sc}$  phase forms, it cannot be re-solutionized. This being the case, it is desirable to limit its formation during casting so that it can be formed homogeneously at a lower temperature as smaller, better distributed precipitates. To maximize the cooling rate, the casting mold fitted with removable copper chill blocks that carry chilled cooling water (Figure 3.3). Taking into account the total heat capacity of the ingot, these blocks were engineered to produce a maximum cooling rate of  $20^\circ\text{C}/\text{second}$ . As heat is removed from the surface it must conduct out from the center. This finite heat conduction within the ingot slows the actual cooling rate relative to the ideal one. Also, the heat transfer between the ingot and the chill blocks reduce the cooling rate. The heat transfer is initially high between the liquid metal and the copper, but it decreases as the ingot freezes and cools.

In order to determine the actual ingot cooling rate, a test ingot was poured into the mold and a thermocouple was immediately inserted into the top to monitor the temperature. This test provided cooling rate information for the top of the ingot. The center of the ingot is expected to freeze at the slowest rate. This simple test confirmed that the actual cooling rate for the top of the ingot was in excess of  $10^\circ\text{C}/\text{second}$  down to about  $550^\circ\text{C}$  (Figure 3.4).

The final problem encountered was the need to fill the mold with metal fast enough to produce a solid ingot. To understand the casting difficulties encountered, an explanation of this procedure is required. After alloying and degassing, casting is initiated by evacuating the plenum area. This creates a pressure differential across the

filter and causes the melt to pass down through the filter and into the mold. During early castings, a problem developed because the metal did not pass through the filter quickly enough to produce a solid ingot. To solve this problem a compromise was made between the degassing efficiency (small bubble size) and the need for rapid casting. When the filter was thinned enough to pass the melt (0.1") it lacked sufficient strength and fractured during casting. The successful design was to thin the filter to 0.2" in the center and then further thin 0.25" circles down to 0.1" while leaving the thicker material for support between them. Finally, several very small holes (.02") were drilled through each of these thinned areas (Figure 3.5). With this final design it was possible to preserve the inert gas flushing and also get the metal into the casting mold fast enough to form a solid ingot.

### 3.3 Melting Procedure

The following section covers in detail the actual operation of the Light Alloy Melting Facility. Prior to each melt the furnace required special preparation in order for it to function as designed. These steps included baking out all of the porous components to remove water and thoroughly flushing the entire facility with dry argon gas. Also, there are two consumable components that must be replaced each melt: the filter and crucible. These required special preparation before each cast.

#### 3.3.1. Carbon Filter

The filters used were made of porous carbon and were obtained from Union Carbide. The starting size was 0.5" thick and 4.5" in diameter. These were sliced half to  $\approx 0.25$ " and then machined to the dimensions previously discussed.

#### 3.3.2. Crucible Design

The crucible is made from two cylindrical tubes of MgO. These are made by machining the bottom off of a 4.5" diameter crucible and then cutting the resulting tube in half; the exact dimensions are given in Figure 3.6. MgO was selected because it is very resistant to attack from aluminum melts that contain lithium. However, it has relatively

poor resistance to thermally induced stress and this causes the lower half of the crucible to crack during the course of casting. By using a two piece crucible, the upper half can be reused, and only a new lower piece must be machined. An interlocking groove is machined into each half-crucible that aligns them and also allows the lower one to expand radially.

### 3.3.3. Furnace Assembly

Prior to assembling the furnace, the porous components (crucible, transition ring) were baked out at 500°C for a minimum of 24 hours. This was necessary to remove any moisture that these parts may have absorbed from the atmosphere. The next step was to assemble the complete furnace and evacuate the containment vessel. From the time the furnace was assembled it was kept under vacuum at all times except to insert the alloy charge.

The furnace assembly procedure begins by placing the two viton o-rings into their grooves in the bottom of the transition ring. This assembly was then inverted on top of the casting mold so that the o-rings seal the bottom of the transition ring to the stainless steel mold. The previously machined filter was then placed onto the transition ring and fitted into the depression cut for it. Next, the crucible assembly was centered on top of the filter and wrapped with an insulating blanket. The induction coil was carefully lowered around this assembly so as not to disturb the alignment of the crucible, filter and transition ring. It also must not catch on the insulating blanket or it will compress it down and cause the induction coil to be off-center. The last step was to clamp the entire assembly together from the top. This was accomplished by placing two insulating spacers on top of the crucible and placing the copper clamp assembly on them. The actual clamping force came from 4 springs with turnbuckles attached to them that extended down outside the induction coil. They were attached to anchoring extensions that protrude out from the casting mold. The turnbuckles are then used to adjust the clamping force that extends down from the top of the crucible, through the filter/transition ring and

into the clamping mold. This clamping force was extremely critical to successful operation of the furnace because it maintains the o-ring seals of the transition region and it keeps the crucible/filter from lifting up off the mold due to the argon pressure used to degas the melt. At this point the furnace was fully assembled and ready to be charged with the alloying metal.

#### 3.3.4. Charge Preparation

The alloy charge for all of the alloys produced for this research consisted of an Al-0.5%Sc master alloy provided by Alcoa. This material was in the form of  $\approx$ 500 gram rods that were placed vertically into the crucible with one end resting on the filter. The lithium alloying addition was added as elemental, alloy grade lithium purchased from Foote mineral. Prior to melting, the desired amount of lithium was carefully weighed, enclosed in common aluminum foil, and hung above the furnace from the alloying control rod. For the magnesium containing alloy, high purity magnesium was added in the form of 1 cm rod that was suspended above the furnace with the lithium. The containment vessel was then sealed and evacuated, flushed with argon and left under vacuum for at least 24 hours.

#### 3.3.5. Melting/Casting

With the furnace fully assembled, charged and dehydrated it was now ready for the melting procedure. Starting with the containment vessel fully evacuated, it was backfilled with dry argon gas to near atmospheric pressure and then evacuated again. This flushing operation was repeated a minimum of three times in order to remove the maximum amount of reactive gases. The induction coil was now energized and power to it increased to produce low power input (4%) to begin warming the Al-Sc rods in the crucible. Because induction heating depends on the resistance heating due to currents induced in the charge, it is least efficient when the metal is cold. However, as the melt warms, the induction becomes more and more efficient. Due to this, the best procedure for melting was to warm the melt at low power inputs and then increase the power by 1%

every 5 minutes. Melting generally occurred at power input of 8% after about 30 to 45 minutes of induction heating.

At the start of melting the pressure in the containment vessel was kept low (<0.5 psi). This helped to remove any gases produced by the melt as it warmed up. During this time the pressure below the filter (plenum) was slightly raised to cause a small flow of argon up through the melt to further remove outgassing from the charge. As melting proceeded the containment vessel pressure was allowed to increase to 5 psi and the plenum pressure was increased to flow more argon through the filter. This also kept the molten alloy from flowing through the filter due to gravity.

As the Al-Sc charge becomes fully molten, the argon flow through it is very carefully adjusted using a sensitive needles valve while viewing the melt through an observation port. If the argon flow is slightly too high, the melt will splash up the side of the crucible and out of the top. Also, this argon flow setting will vary depending on the absolute pressure inside of the containment vessel, with more flow required as the vessel pressure increases. After 5 minutes of this mixing, the alloying elements were lowered into the melt from above using the control rod. Due to the exothermic reaction of the lithium with the melt, the induction power was lowered 2% as the lithium was added and the argon flow rate was maximized to rapidly distribute the lithium. During all this time the vessel pressure was maintained between 5 and 8 psi.

With the charge fully molten and alloyed, the final degassing prior to casting was performed. For this the argon flow was increased to the maximum allowable without excessive splashing and the induction power was adjusted so that the melt had a strong red glow. These parameters were maintained for approximately 10 minutes under careful observation through the view port. At this time, the pressure within the containment vessel was allowed to increase to 9 psi and the induction power was reduced slightly (2%) in preparation for casting. To initiate casting, the flow of argon to the plenum was stopped and vacuum was applied through a gate valve and mechanical vacuum pump.



This pressure gradient across the filter causes the alloy to flow down into the casting mold. It was critical at this time that the metal flow into the mold in a timely fashion so that it formed a solid ingot. Due to the rapid cooling rate, it was possible for the metal to freeze into a globular metal/air composite if the fill rate is too slow. Satisfactory castings were accomplished when the entire melt passed into the mold in less than 30 seconds. As mentioned in the filter preparation section, this required a balance between the filter thickness and the pressure differential applied across it. Lastly, as the metal level dropped near the filter, the induction power must be turned down to keep the filter from taking the full induction field. This would cause it to overheat and collapse as the casting operation nears completion.

### 3.4. ALLOYS PRODUCED

A total of four ingots were cast by the author for this research project. Each weighed approximately 1 kilogram and had approximate dimensions 7 x 3.5 x 1.75 inches. The composition in weight percent of these ingots are given in Table 3.1.

Table 3.1. Elemental compositions of alloys produced in weight percent (atomic percent in parentheses).

Alloy	Li	Sc	Mg	Cu	Fe
ALS0	0	0.5 (0.3)	0.01	0.01	0.005
ALS1	1.1 (4.2)	0.5 (0.3)	0.01	0.01	0.03
ALS2	2.2 (8.0)	0.5 (0.3)	0.01	0.01	0.03
ALS4	2.0 (7.3)	0.5 (0.3)	2.1 (2.3)	0.01	0.04

## 4. EXPERIMENTAL PROCEDURE

### 4.1. Thermomechanical Processing

Metal alloys not intended for use in the as-cast condition are normally subjected to a sequence of mechanical deformations and thermal excursions. This sequence of treatments is commonly referred to as thermomechanical processing and is intended to modify the initial microstructure through a combination of effects: grain deformation leading to recrystallization or subgrain formation, initial precipitate dissolution or redistribution, or precipitation of second phases. It is also used to produce a product (such as sheet or plate) from the initial ingot. The thermomechanical processing of the alloys studied in this research served two purposes: it converted the ingot into sheet form appropriate for test samples, and it modified the as-cast microstructure into one that is superplastically deformable.

#### 4.1.1. Low Lithium Alloys

The thermomechanical processing used for alloys ALS0 and ALS1 was similar to the procedure developed by Alcoa for their Al-Sc-Mg alloys. The procedure consisted of warm rolling at 275°C, cold rolling, and a final aging treatment also at 275°C. The majority of the scandium precipitates out as Al<sub>3</sub>Sc during warm rolling and the final aging step produces only a slight increase in strength.

#### 4.1.2. High Lithium alloys

The addition of larger amounts of lithium (>1.4%) forces a significant modification of the thermomechanical processing. An examination of the Al-Li binary phase diagram (Figure 2.2) reveals that two intermetallic phases can form at the aluminum-rich end of this system: Al<sub>3</sub>Li ( $\delta'$ ) and AlLi ( $\delta$ ). At lower temperatures (<280°C),  $\delta'$  forms and strengthens the alloy such that only limited rolling can be

performed before severe cracking occurs. At higher temperatures ( $280^{\circ}\text{C} < T < 425^{\circ}\text{C}$ ) the phase  $\delta$  (AlLi) forms and can be a serious problem because it nucleates heterogeneously on grain boundaries and is exceptionally brittle<sup>30</sup>. This phase has been identified as promoting grain boundary failure in Al-Li alloys<sup>31</sup>.

As a result, most Al-Li alloys are processed at above the lithium solvus temperature to avoid rolling failures from the  $\delta$  phase. However, in scandium containing alloys, it is desired to limit the materials exposure to high temperatures because of overaging of the  $\text{Al}_3\text{Sc}$  precipitates. With this in mind, two initial rolling temperatures were selected:  $350^{\circ}\text{C}$  (designated WR) and  $500^{\circ}\text{C}$  (designated HR). Figure 4.1 is a schematic diagram of the complete HR and WR process. The advantage of the WR processing was that less overaging of the  $\text{Al}_3\text{Sc}$  precipitates occurred and this should produce a higher strength material. However, at  $350^{\circ}\text{C}$  there was much more danger of edge cracks that propagate through the material and these were removed between rolling steps before they reached a critical size. The cause of this cracking was the presence of the  $\delta$  phase and the higher flow stress of the material at  $350^{\circ}\text{C}$ .

The WR process, since it occurred in the two phase region, resulted in the formation of large quantities of  $\delta$  and this was verified using X-ray diffraction. To eliminate this phase, the WR alloys were all given a solution heat treatment prior to aging. The HR alloys were also given a solution heat treatment because during rolling the material cooled below the  $\delta$  solvus before it could be quenched and X-ray diffraction identified the presence of  $\delta$ .

In determining the solution heat treating parameters it was desired to minimize the exposure of the material to high temperature. To accomplish this, test samples were exposed to 1 hour at 400, 450, and  $500^{\circ}\text{C}$ . The samples were checked for the presence of  $\delta$  with X-ray diffraction. The sample solution heat treated at  $450^{\circ}\text{C}$  showed little  $\delta$ , however when it was aged to peak strength ( $170^{\circ}\text{C}$  for 20 hours) a large amount of  $\delta$  formed. This indicated that  $\delta$  nuclei remained in the material and were able to grow at the

low temperature aging. The same procedure was used on the 500°C material and little  $\delta$  was found even after aging at 170°C. It was concluded that this was the minimum solution heat treatment temperature required and it was used for all subsequent solution heat treatments.

#### 4.1.3. High Lithium Alloys with Magnesium

The thermomechanical processing of Alloy ALS4 was the same as that used for ALS2 at high temperature (HR) but was modified for the warm rolling (WR). As for ALS2, the HR procedure consisted of hot rolling at 500°C followed by a 1 hour solution heat treatment at 500°C. For the WR process, it was found that ALS4 would tolerate some cold rolling alternated with warm rolling (350°C) in the initial ingot breakdown. Then, as the reduction in thickness exceeded 2:1, the strength of the ingot became too high for cold rolling. The remaining rolling was all performed at 400°C. The WR temperature was increased to 400°C because during the rolling of ALS2 it was determined that 350°C was pushing the limits of ingot cracking. A schematic diagram of the actual WR process used on ingot ALS4 is Figure 4.2.

When X-ray Diffraction was performed on the WR-ALS4 alloy there was very little  $\delta$  observed, instead the ternary S ( $\text{Al}_2\text{LiMg}$ ) phase was found. In light of this, it was decided that the solution heat treatment could be eliminated and the alloy was aged directly after rolling.

#### 4.2. Mechanical Testing

Two methods of strength characterization were used in this research: Rockwell Hardness tests (A and K scales) and uniaxial tensile tests on subsize (1" gage) samples (Figure 4.3). Hardness testing was used during rolling and solution heat treating to understand the effect of each processing step on the alloy's strength. It was then used to determine the aging parameters (time, temperature) to achieve peak strength. After this,

tensile tests were performed at room (300 K) and liquid nitrogen (77 K) temperature to determine the yield strength (0.2% offset), ultimate tensile strength and total plastic elongation of the peak aged material.

Tensile testing was performed using a computer controlled, hydraulic testing machine configured to allow cryogenic testing. A clip-on extensometer with 1" gage length was used for each test to directly monitor the strain of the sample. All tests were performed at a fixed strain rate of  $\approx 2\%$ /minute. All data was collected digitally on the controlling computer for subsequent analysis.

Tests of ALS0 and ALS1 were performed on warm rolled (275°C) + cold rolled + peak aged material. The results of these tests are given in Table 4.1 with data reported by Alcoa for their Al-0.5%Sc alloy.

Alloy ALS2 was tested for two rolling conditions: hot roll (500°C) + solution heat treatment (500°C/1hour) + peak age and warm roll (350°C) + solution heat treatment (500°C/1hour) + peak age. The results of these tests are given in Table 4.2. For comparison, Table 4.2 also contains data on Al-Li-Zr alloys from two other researchers.

Alloy ALS4 was tested for two different rolling conditions: hot roll (500°C) + solution heat treatment (500°C/1hour) + peak age and warm roll (400°C) + peak age. The results of these tests are in Table 4.3 along with data from other researchers on comparable alloys.

Table 4.1. Tensile test results of ALS0 and ALS1 along with data reported by Alcoa for their Al-0.5Sc alloy.

Alloy	Condition	Test Temp. K	TYS MPa (ksi)	UTS MPa (ksi)	% Elongation
ALS0	WR+CR+AGE	300	215 (31)	220 (32)	14
		77	240 (35)	340 (49)	35
ALS1	WR+CR+AGE	300	265 (38)	305 (44)	9
		77	310 (45)	400 (58)	30
Al-0.5Sc Alcoa <sup>3233</sup>	WR+AGE	300	285 (41)	295 (43)	14.5

Table 4.2. Tensile test results of ALS2 along with data reported by other researchers on Al-Li-Zr alloys.

Alloy	Condition	Test Temp. K	TYS MPa (ksi)	UTS MPa (ksi)	% Elongation
ALS2	HR+SHT+A	300	354 (50)	441 (64)	7
		77	360 (51)	552 (80)	16
ALS2	WR+SHT+A	300	372 (54)	441 (64)	6
		77	380 (55)	560 (81)	12
Glazer <sup>34</sup> (hot rolled, SHT (1hour at 555°C), stretched 2%, aged 7 hours at 190°C)					
Al-2.4Li-0.1Zr		300	275 (40)	345 (50)	3
		77	270 (39)	420 (61)	11
Dinsdale <sup>35</sup> ( extruded, SHT and aged 16 hours at 170°C)					
Al-2.0Li-0.2Zr		300	240 (35)	334 (48)	6

Table 4.3. Tensile test results of ALS4 along with data reported by other researchers on Al-Li-Mg-Zr and Al-Sc-Mg alloys.

Alloy	Condition	Test Temp. K	TYS MPa (ksi)	UTS MPa (ksi)	% Elongation
ALS4	HR+SHT+A	300	345 (50)	462 (67)	8.5
		77	360 (52)	586 (85)	21
ALS4	WR+A	300	428 (62)	503 (73)	9
		77	483 (70)	610 (88)	17
Alcoa (warm rolled at 288°C, aged at 288°C for 4 hours) <sup>3637</sup>					
Al-0.5Sc-2.0Mg	Wr	300	341 (49)	370 (54)	13.5
Dinsdale <sup>38</sup> ( extruded, SHT and aged 16 hours at 170°C)					
Al-2.0Li-2.0Mg-0.2Zr		300	334 (48)	442 (64)	5

#### 4.3. Slip Line Traces

To study the slip line traces that formed during deformation, tensile blanks of ALS2 (HR+SHT+Age) and ALS4 (HR+SHT+Age) were polished for metallographic examination prior to testing at 300 K and 77 K. Slip lines are formed on the surface of polished test samples when crystallographic planes undergoing shear intersect the surface. These provide us with information on the distribution of slip that is occurring in the metal. After testing, the samples were examined using optical and scanning electron microscopy to study the slip lines formed.

#### 4.4. Fracture Surfaces

The fracture surfaces of the tensile specimens tested for the slip line analysis were examined using scanning electron microscopy. This provided information on any difference in fracture mode between the two alloys at 300K and 77K.

## 5. DISCUSSION

### 5.1. Microstructure Characterization

#### 5.1.1. As-Cast Material

In the as-cast condition alloys ALS2 and ALS4 have a fine, equiaxed grain structure with an average grain diameter of 35  $\mu\text{m}$  and 25  $\mu\text{m}$  respectively. Optical micrographs for both alloys are included as Figure 5.1. An examination of the as-cast material using differential scanning calorimetry (DSC) was made by increasing the temperature from 50°C to 550°C at a rate of 40°C/minute and monitoring the heat flow. The sample is then cooled rapidly, stabilized at 50°C and ramped to 550°C again. This sequence was repeated again for a total of three runs on a single sample. When this series of DSC scans was performed on the as-cast alloys (Figure 5.2), it is found that the scandium remaining in solution precipitates out on the initial run, but not on subsequent ones. This indicates that the cooling rate of the ingot was sufficient to keep some of the scandium in solution. Also observed is that the amount of lithium precipitating out at low temperature as  $\text{Al}_3\text{Li}$  is minimized on the first run. This indicates that some of the lithium is already incorporated into intermetallics ( $\delta$  and  $\delta'$ ) in the as-cast material and that these dissolve during the first exposure to high temperature. The presence of both  $\delta$  and  $\delta'$  in the as-cast alloys was confirmed by X-ray Diffraction.

#### 5.1.2. Rolled Sheet

The rolled microstructure is fully unrecrystallized with elongated grains and a uniform distribution of  $\text{Al}_3\text{Sc}$  precipitates. These dispersoids pin the grain boundaries, preventing grain growth or recrystallization. This effect is observed in transmission electron microscopy as grain boundaries that have bowed out around  $\text{Al}_3\text{Sc}$  dispersoids (Figure 5.3). There is a slight difference between the two alloys in this condition (Figure 5.4); ALS4 has developed what appears to be a finer grain structure. The grain size of alloy ALS2 is approximately 150 x 50 x 10  $\mu\text{m}$  and of ALS4 is 40 x 25 x 5  $\mu\text{m}$ .



After the rolling of alloys ALS2 and ALS4, a large volume fraction of an unknown phase was observed in as-polished optical specimens (Figure 5.5). It was found that this phase would form in the as-cast material (Figure 5.5) after exposure to relatively low temperatures (350°C/48 hours). EDS analysis in the SEM indicated that the only detectable elements in this phase were aluminum and scandium. Henceforth, this phase will be referred to as  $\nu$ .

#### 5.1.2.1. Melting Study

Using DSC it was possible to determine the melting temperature of the rolled alloys. This is done by heating a sample in a graphite pan from 50°C to 600°C at a rate of 40°C/minute. The sample is then heated from 600°C to melting at a rate of 2°C/minute. This slow heating rate allows time for solute homogenization and gives an accurate value for the onset of melting. In addition to samples of the Al-Li-Sc alloys, a sample of Al-2.4Li-0.1Zr was also tested as a standard. The melting temperatures found are given in Table 5.1. The data for alloy ALS2 does not fit with the other alloys; it melted at a lower temperature than was expected. This can be seen by plotting the results obtained with the commonly accepted Al-Li phase diagram (Figure 5.6). One possible explanation for this effect is that the unknown phase ( $\nu$ ) is a ternary Al-Sc-Li eutectic phase that has a lower melting point than Al-Li alloys that do not contain scandium.

Table 5.1. Melting temperature of alloys determined by Differential Scanning Calorimetry.

Alloy	Al	Li	Sc	Zr	Melting Temperature (°C)
ALS0	bal	0	0.5	0	660
ALS1	bal	1.1	0.5	0	658
ALS2	bal	2.2	0.5	0	640
Al-Li (Glazer)	bal	2.4	0	0.1	648

### 5.1.2.2. Phase Equilibrium Study

To study  $v$  phase, along with the others present in this system, rolled sheet samples of both high lithium alloys were subjected to long heat treatments (24-48 hours) at the following temperatures: 350, 400, 450, 500, and 550°C. Optical micrographs of the resulting microstructures of these samples are Figures 5.7 and 5.8. The most striking observation is that the  $v$  phase is present in all samples at roughly the same quantity, size, and distribution. The samples were then examined using X-ray diffraction. A summary of the phases identified for each temperature is presented in Table 5.2. The X-ray diffraction of the higher temperature samples indicated only weak  $L1_2$  peaks, leading to the conclusion that  $v$  exists in that structure. This is surprising because a lithium containing compound would be expected to solutionize and scandium containing precipitates have not been previously observed in the morphology or size of  $v$ . In all other studies of Al-Sc alloys, the  $Al_3Sc$  phase is found as a very small, coherent precipitate with a round shape.

Table 5.2. Phases identified by X-ray diffraction in overaged alloys.

Alloy	Temp. (°C)	$\delta'$ or $v$ ( $L1_2$ )	$\delta$ (AlLi)	S ( $Al_2LiMg$ )
ALS2	350	weak	very strong	-
	400	weak	moderate	-
	450	weak	very weak	-
	500	weak	none	-
	550	weak	none	-
ALS4	350	weak	weak	moderate
	400	weak	very weak	weak
	450	weak	none	none
	500	weak	none	none
	550	weak	none	none

An attempt was made to precipitate the  $\nu$  phase in alloys that did not contain lithium and this proved unsuccessful. Several samples of non-lithium alloys were exposed to high temperature (550°C) for times up to 200 hours. In this condition, the  $\text{Al}_3\text{Sc}$  phase could be resolved and identified in the scanning Auger microscope after sputtering the surface (Figure 5.9). However, the size and quantity of the  $\text{Al}_3\text{Sc}$  phase was still much smaller than that of the  $\nu$  phase observed in lithium containing alloys. It was also observed to remain in a spherical morphology, while  $\nu$  forms into multi-faceted polyhedrons (Figure 5.10). This led to the tentative conclusion that  $\nu$  is an ordered  $\text{L1}_2$  phase containing scandium and lithium. To verify the presence of lithium and attempt to determine the Sc:Li ratio, quantitative scanning Auger microscopy was used. Details of this analysis are included as Appendix 1.

The results of a typical analysis is given in Table 5.3 and indicate that the precipitate composition is approximately  $\text{Al}_3(\text{Li}_{0.5}\text{Sc}_{0.5})$ . This result was consistent for all of the Auger spectra obtained. At this time it should be pointed out that these results represent the lower bound of the lithium concentration because of the difference in precipitate sizes. The  $\text{Al}_3\text{Sc}$  precipitates, used as the standard, were only slightly larger than the Auger probe size. This makes it difficult to insure that all of the Auger electrons collected came from the  $\text{Al}_3\text{Sc}$  phase. If they are not, the assumption of stoichiometry ( $X_{\text{Al}} = 0.75$ ,  $X_{\text{Sc}} = 0.25$ ) becomes invalid since some of the material sampled would be pure aluminum and later calculations would yield artificially high values of  $X_{\text{Sc}}$ . This problem did not occur with the  $\nu$  phase because its size was several times larger than the probe, allowing accurate collection from only the precipitate.

It is believed that  $\nu$  actually contains less scandium than was calculated using the Auger technique. This is because the amount of  $\nu$  present ( $\approx 2.5$  volume %) at the proposed composition ( $\text{Al}_3\text{Li}_{0.5}\text{Sc}_{0.5}$ ) would account for all of the scandium in the material. However, using transmission electron microscopy, small precipitates of  $\text{Al}_3\text{Sc}$

are observed to be distributed throughout the microstructure (Figure 5.3). This indicates that all of the scandium is not being used to form  $\nu$ .

The results of this study provide a possible solution to the decreased melting temperature of the Al-Li-Sc alloys that was seen using DSC. It appears from this data that  $\nu$  ( $\text{Al}_3(\text{Sc},\text{Li})$ ) is a ternary eutectic phase that is lowering the solidus temperature of the high lithium alloys.

Table 5.3. Results of quantitative Auger study of  $\text{Al}_3(\text{Sc},\text{Li})$  precipitates in alloy ALS2.

Collection Parameters: $E_p = 5\text{KeV}$ $I_p = 4.0 \text{ nA}$			
Sample	Collected Intensities		Calculated Relative Sensitivity
Standard- $\text{Al}_3\text{Sc}$	$I_{\text{Al}} = 20$	$I_{\text{Sc}} = 35$	$S_{\text{Sc}} = 5.25$
Unknown- $\text{Al}_3(\text{Sc},\text{Li})$	$I_{\text{Al}} = 44$	$I_{\text{Sc}} = 40$	$I_{\text{Li}}/S_{\text{Li}} = 7.05$

Calculated Atomic Fraction of Scandium in  $\text{Al}_3(\text{Sc},\text{Li})$ -  $X_{\text{Sc}} = 0.13$

#### 5.1.4. Aging

The aging parameters to achieve peak strength were determined using Rockwell Hardness measurements of samples that had received a solution heat treatment and water quench. These samples were aged at  $150^\circ\text{C}$  and  $170^\circ\text{C}$  in a circulating air heat treating furnace and water quenched prior to testing. From these experiments it was determined that 20 hours at  $170^\circ\text{C}$  produced the maximum strength.

## 5.2. Mechanical Properties

These alloys are targeted for use as superplastically formed complex structures for weight critical applications. As such, the optimal characterization of mechanical properties of these alloys would be performed on superplastically formed material that is appropriately aged. However, this testing was not possible during this initial

development project and will likely be performed in subsequent research<sup>39</sup>. The mechanical testing that was performed was on rolled and peak aged material. The goal is to understand the potential of these alloys for strength and ductility so that this can be compared with the ternary systems (Al-Li-Mg and Al-Sc-Mg) that the Al-Li-Sc-Mg alloys are based on. This information can then be used as an upper limit to the possible post-superplastically formed mechanical properties. Due to a limited supply of material, no attempt has been made to study the fracture toughness or fatigue properties of these alloys. This testing would certainly be necessary if development of these alloys is continued.

#### 5.2.1. Aluminum-Scandium

The strength of ALS0 is somewhat lower than what Alcoa reported for their Al-0.5Sc alloy. There are two reasons for this: the cooling rate was not as rapid and it was not cold worked to the same extent as Alcoa's alloy was. The slower cooling rate is probably the most important difference since it allowed a greater amount of Al<sub>3</sub>Sc to form on casting. This results in precipitates larger than the optimum size ( $\approx 7$  nm<sup>40</sup>) and reduces the maximum strength achievable. Since the scandium cannot be re-solutionized, any precipitates larger than the optimum size reduces the strength achievable. The slower cooling rate is due to the fact that the Light Alloy Melting Facility was constructed for producing Al-Li alloys; thus it was not possible to direct chill cast into water as Alcoa did with their Al-Sc alloys. Secondly, the amount of cold work that could be imparted on ALS0 was significantly less than that done on Alcoa's material due to a thinner starting ingot.

#### 5.2.2. Aluminum-Scandium-Lithium

The lithium content of ALS1 is too low to form  $\delta'$  so its strength comes from Al<sub>3</sub>Sc precipitates, grain boundaries, cold work and lithium in solid solution. The processing of ALS2 requires the use of higher temperatures and this causes overaging of the Al<sub>3</sub>Sc precipitates. Also, no cold work was used since it is not possible to cold work

superplastically formed parts. In spite of this, the strength of ALS2 is significantly (>40%) higher than ALS1. This strength increase is caused by the  $\delta'$  ( $\text{Al}_3\text{Li}$ ) that is formed in this alloy during aging at low temperature (170°C).

To reduce the overaging of the  $\text{Al}_3\text{Sc}$  precipitates, ALS2 was also rolled at 350°C (WR). A comparison of the results for ALS2-HR and ALS2-WR alloys indicates that this was successful; there is an 8% increase in yield strength for the WR material. The solution heat treatment and aging of these alloys was the same leading to similar  $\delta'$  strengthening. The only microstructural difference is less overaging of the scandium precipitates.

A comparison of ALS2 with the Al-Li-Zr alloys (Figure 5.11) shows that both the strength and ductility of Al-Li-Sc alloys are superior. The increased strength can be attributed to the following factors: effective grain size and strengthening from  $\text{Al}_3\text{Sc}$  precipitates. The improved ductility is believed to be caused by a reduction in the stress concentration at grain boundaries because ALS2 has a shorter effective slip distance. The grain size reported by Glazer for the Al-2.4Li-0.2Zr alloys was 1000 x 250 x 45  $\mu\text{m}$  which is considerably larger than that of ALS2 (150 x 50 x 10  $\mu\text{m}$ ).

There is little difference in the yield strengths of the ALS2 samples tested at 300 K and 77 K. This is also true for the Al-Li-Zr alloy studied by Glazer. When  $\delta'$  is sheared by a unit dislocation an antiphase boundary is formed. This increases the energy of the material and accounts for the strengthening contribution of  $\delta'$ . This antiphase boundary energy is relatively insensitive to temperature and because of this the yield strengths of non-cold worked Al-Li alloys does not dramatically increase with decreasing temperature.

There is a large increase in elongation to failure and a corresponding increase in ultimate tensile strength at 77 K. The reason for this is a change in the deformation behavior that causes less slip localization. This was confirmed by examining slip line tracings and is discussed in a subsequent section.

### 5.2.3. Aluminum-Scandium-Lithium-Magnesium

The thermomechanical processing of ALS4-HR was the same as that given to ALS2-HR. The yield strengths of these conditions were the nearly same but ALS4 exhibited better elongation and ultimate strength. The thermomechanical processing of both of these samples included a solution heat treatment and this resulted in similar overaging of the  $Al_3Sc$ . Magnesium is expected to give ALS4 a strength increase from solid solution strengthening, but less lithium is available for formation of  $\delta'$ . Since approximately 5 at.% lithium remains in solid solution, alloys ALS2 and ALS4 have 3 at.% and 2.3 at.% respectively available for precipitation. This reduction in  $\delta'$  is countering the effects of magnesium in solid solution and the result is similar strengths for both alloys in the HR condition. This changes dramatically when the WR conditions are compared.

The mechanical properties of ALS4-WR are significantly better than any of the other alloys. The key to these property improvements was the elimination of the solution heat treatment. The result is that 400°C is the highest temperature that this alloy was exposed to and this limited the overaging of the  $Al_3Sc$ . Also, some cold rolling was possible early in the rolling of this alloy and this, along with the presence of magnesium, allowed this material to develop a finer microstructure and thus greater ductility by limiting the effects of slip localization.

It is of interest to compare ALS4-WR with two other alloys: Alcoa's warm rolled Al-0.5Sc-2.0Mg and Dinsdale's Al-2.0Li-2.0Mg-0.2Zr. These two alloys have nearly identical yield strengths that are >25% lower than ALS4-WR. Also, the elongation to failure of ALS4-WR at 9% is much better than the 5% reported for the Al-2.0Li-2.0Mg-0.2Zr alloy. This indicates that the addition of scandium is producing a much more ductile Al-Li alloy than is possible with zirconium, and at much higher strength levels.

### 5.3. Slip Line Traces

For all of the samples, it was observed that the slip lines did not cross grain boundaries. This is in contrast to other Al-Li alloys (2090) where the slip lines are seen to extend across several grains<sup>41</sup>. The slip lines for alloys ALS2 and ALS4 at 300 K were relatively widely spaced, indicating that deformation is localizing on a small number of slip planes. In alloy ALS2, the slip lines were generally straight as they ran across the grain (Figure 5.12). However, in the magnesium containing alloy, the slip lines were not straight, appearing to change direction every 5 to 10 microns (Figure 5.12). There are two possible explanations for this behavior: the presence of S ( $\text{Al}_2\text{MgLi}$ ) phase that is non-shearable, forcing a change in slip system, or the development of subgrains with sufficiently high angle boundaries that they change the slip system.

A distinct difference in slip traces at 300K and 77K is seen for both alloys. At the lower temperatures, the slip step height is reduced and the traces are much more finely spaced (Figure 5.13). This change in the slip characteristics indicate that the deformation at 77 K is much less localized than that occurring at 300 K. This reduces the stress concentrations that exist at grain boundaries and this is responsible for the improved elongation of samples tested at 77K.

### 5.4. Effect of Deformation on $\nu$ phase.

The examination of the polished tensile specimens provided the opportunity to observe the effect of deformation on  $\nu$  phase ( $\text{Al}_3(\text{Sc,Li})$ ) present in these alloys. As expected, slip lines did not cross through the regions containing  $\nu$  phase. Instead, it was found that when plastic strain reached about 4%, the  $\nu$  phase began to fracture (Figure 5.14). This effect was completely independent of alloy or test temperature.

The result of these fractured precipitates is that the material would now contain a distribution of internal cracks. Therefore, the difference in elongation between the



samples tested was dependent on the ability of the material to continue to deform in the presence of the defects without fracturing.

### 5.5. Tensile Fracture Surfaces

For samples tested at 300 K there was little or no difference between the fracture surfaces of ALS2 and ALS4 (Figures 5.15 and 5.16). They can both be classified as a combination of ductile rupture and transgranular cleavage. At 77 K the fracture mode of both alloys changes to almost totally ductile rupture (Figures 5.17 and 5.18). From the slip line study it was seen that deformation is more uniformly distributed in samples tested at 77 K. This is consistent with the reduction in cleavage seen in the low temperature fracture surfaces.

## 6. SUMMARY

The mechanical properties of Al-Li-Sc and Al-Li-Sc-Mg alloys are much better than corresponding alloys that utilize zirconium for microstructure stabilization. The reason for this is that scandium containing alloys have a smaller effective grain size and this reduces the slip distance between dislocation blocks (grain boundaries). Since slip localization leads to failure in Al-Li alloys, reducing the slip distance has the effect of reducing the stress concentration at grain boundaries that lead to fracture. The properties for alloy ALS4 are especially promising as they approach those of the best superplastically formable aluminum alloy currently available.

In alloys containing scandium and greater than 2.0% lithium, there is a ternary eutectic phase ( $\nu$ ) that forms on casting. This phase has the same structure as  $\text{Al}_3\text{Li}$  and  $\text{Al}_3\text{Sc}$  (ordered  $\text{L1}_2$ ) with a lattice parameter nearly identical to that of aluminum. Scanning Auger microscopy indicates that the volume fraction of scandium is no greater than 0.13 and that lithium accounts for the balance of solute in the  $\text{Al}_3(\text{Sc},\text{Li})$  phase.

This  $\text{Al}_3(\text{Sc},\text{Li})$  phase does not appear to be affected by any of the thermomechanical processing that was performed on the alloys. It begins to fracture after only about 4% plastic deformation and the cracks that form eventually lead to fracture after a large amount of elongation.

### 6.1. Early Superplastic Data

Research into the superplastic properties of these alloys is being performed by another student, E. Bradley. Initial data on this material are promising; elongations up to 1000% have been obtained for alloy ALS4 at 500°C. The mechanism of this behavior is of great interest. It appears that the rolled microstructure undergoes a change in substructure when it is deformed at elevated temperature. This new microstructure is made up of equiaxed grains with diameters of approximately 5  $\mu\text{m}$ . This new grain

structure contains low-angle boundaries, which has not been observed very often after such large amounts of superplastic deformation.

## 7. RECOMMENDATIONS FOR FUTURE WORK

The Al-Sc-Li-Mg system shows great promise for developing low density, superplastically formable structural alloys. A continuation of this work should explore alloys with more magnesium and less lithium. It would be of interest to produce an alloy with a lithium content of  $\approx 1.6\%$  and a magnesium content of  $\approx 4\%$ . This alloy would still be precipitation hardenable with  $\delta'$  but should form less  $\nu$  phase. This would be expected to improve the ductility of the alloy. It could also be processed at lower temperatures without the difficulties of  $\delta$  formation.

## 8. ACKNOWLEDGMENTS

This research was funded by the Director, Office of Energy Research, Office of Basic Energy Science, Materials Sciences Division of the U.S. Department of Energy under Contract No. DE-AC03-76SF00098. The Al-Sc master alloy used to produce the ingots studied was supplied by the Aluminum Company of America.

## 9. REFERENCES

- 1 Wadsworth, J., Pelton A.R., and Lewis R.E., "Superplastic Al-Cu-Li-Mg-Zr Alloys," *Met. Trans.*, 16A, pp. 2319-2332, 1985.
- 2 Grimes, R. and Butler, R.G., "The Forming Behaviour of Commercially Available Superplastic Aluminium Alloys", Superplasticity in Aerospace, eds. H.C. Heikkinen and T.R. Mcnelley, TMS-AIME, Warrendale, PA, 1988.
- 3 Sawtell, R.R. and Jensen, C.L., Mechanical Properties and Microstructure of Al-Mg-Sc Alloys, *Met. Trans.*, 21A, pp. 421-430, 1990.
- 4 Dritz, M.E., Ber, L.B., Bikov, J.G., Toropova, L.S., Anastasieva, G.K., *Fiz. Met. i Metalloved.*, 57, p. 1172, 1984.
- 5 Dorn, J.E., Pietrokowsky, P., and Tietz, T.E., "The Effect of Alloying Elements on the Plastic Properties of Aluminum Alloys", *J. of Metals*, July,
- 6 Boeing, "Low Density Aluminum Alloy Development", First Interim Technical Report, June 1982.
- 7 Private communication E.Bradley.
- 8 Dritz, M.E., Topopova, L.S., and Bykov, Yu.G., *Metallovedenie. i Termicheskaya. Obbrabotka. Metallov*, 1983, vol. 7, pp 60-63.
- 9 Elagin, V.I., Zakharov, V.V., and Rostova, T.D., *Metallovedenie. i Termicheskaya. Obbrabotka. Metallov*, 1983, vol. 7, pp 57-60.
- 10 Blake, N. and Hopkins, M.A., *J. Mat. Sci.*, 1985, vol. 20, pp2861-2867.
- 11 Sawtell, R.R., Bretz, P.E. and Jensen C.L., U.S. Patent 4,689,090, 1987.
- 12 Flower, H.M. and Gregson, P.J., "Solid state phase transformations in aluminium alloys containing lithium," *Materials Science and Technology*, 3, pp. 81-90, February 1987.
- 13 Lavernia, E.J., Srivatsan, T.S., and Mohamed, F.A., "Strength, deformation, fracture behavior and ductility of aluminium-lithium alloys," *Journal of Material Science*, 25, pp. 1137-1158, 1990.
- 14 Khachatryan, A.G., Lindsey, T.F., and J.W. Morris, Jr., "Theoretical Investigation of the Precipitation of delta' in Al-Li," *Met. Trans.*, 19A, pp. 249-258, 1988
- 15 Valentine, M.G. and Sanders, T.H., "The influence of Temperature and composition on the distribution of delta' (Al<sub>3</sub>Li), Aluminum-Lithium 5, eds. Sanders, T.H. and Starke, E.A., Materials and Component Engineering Publications Ltd., Birmingham, UK, 1989.
- 16 Sanders, T.H., "Development of An Al-Mg-Li Alloy" Final Report, 1976.
- 17 Jensrud, O., "Hardening Mechanisms and Ductility of an Al-3.0 wt.%Li Alloy", *Mater. Sci. and Eng.*, 1984.

- 18 Furukawa, M., Miura, Y. and Nemoto, M., "Strengthening Mechanisms in Al-Li Alloys Containing Coherent Ordered Particles", *Japan Institute of Metals*, 26, no.4(1985), pp. 230-235
- 19 Glazer, J., Nieh, T.G., Wadsworth, J. and Morris, J.W., Jr., "Mechanical behavior of superplastically-formed Al-Cu-Li-Zr alloy," MRS Superplasticity symposium, 1988.
- 20 Miller, W.S. and White, J., "The Development of Superplastic 8090 and 8091 Sheet", Superplasticity in Aerospace, *ibid*, pp. 211-228
- 21 F.W. Gayle, "The Development of Aluminum-Lithium Alloys," Naval Air Systems Command Contract No. N00019-78-C-0485, Reynolds Metals Co., Final Report, July 31, 1980.
- 22 *ibid* 5
- 23 *ibid* 3
- 24 Fridlyander, I.N., Sandler, V.S., and Nikol'skaya, T.I., "Change in the Phase Composition of Alloy 01420 During Aging", *All-Union Scientific Research Institute of Aviation Materials*, pp. 2-5, May, 1971.
- 25 Shchegoleva, T.V., and Rybalko, O.F., "Structure of the Metastable S'-Phase in Alloy Al-Mg-Li", *Fiz. Met. i Metalloved.*, 50, no.1, 1980, pp.86-90.
- 26 Metals Handbook Ninth Edition, "Casting", 1988, pp. 85-86
- 27 Boeing "First Interim Technical Report"
- 28 Vasudevan, A.K., Miller, A.C., and Kersker, M.M., "Contribution of Na-Segregation to Fracture Behavior of Al-11.4at.% Li Alloys," unknown book
- 29 Vaynblat, Yu.M., Kopeliovich, B.A., and Golder, Yu.G., "Subboundary Embrittlement of the Alloy Al-Mg-Li by Horophile Impurity Sodium," *Fiz. metal. metalloved.*, 42, no.5, pp. 1021-1028, 1976.
- 30 Huang, T.S. and Brittain, J.O., "The Mechanical Behavior of b-LiAl", *Materials Science and Engineering*, 93, pp. 93-97, 1987.
- 31 Vasudevan, A.K., Ludwiczak, E.A., Baumann, S.F., Doherty, R.D., and Kersker, M.M., "Fracture behavior in Al-Li alloys: role of grain boundary d," *Materials Science and Engineering*, 72, pp. 25-30, 1985.
- 32 *ibid* 3.
- 33 Verzasconi, S.L., "Cryogenic Mechanical Properties of Low Density Superplastic Aluminum Alloys," M.S. Thesis, University of California, Berkeley, May 1989.
- 34 Glazer, J., PhD Thesis, "The Strength-Toughness Combination of the Al-Li alloys 2090 and 2091 at Cryogenic Temperatures", University of California, Berkeley, July 1989.

- 35 Dinsdale, K., Harris, S.J., and Noble, B., "Relationship Between Microstructure and Mechanical Properties of Aluminum-Lithium-Magnesium Alloys," Aluminum-Lithium Alloys, eds. T.H. Sanders, Jr. and E.A. Starke, Jr., TMS-AIME, Warrendale, PA, 1981.
- 36 *ibid* 3.
- 37 *ibid* 30.
- 38 Dinsdale, K., Harris, S.J., and Noble, B., "Relationship Between Microstructure and Mechanical Properties of Aluminum-Lithium-Magnesium Alloys," Aluminum-Lithium Alloys, eds. T.H. Sanders, Jr. and E.A. Starke, Jr., TMS-AIME, Warrendale, PA, 1981.
- 39 Private communication with E. Bradley, Lawrence Berkeley Laboratory.
- 40 *ibid* 4
- 41 *ibit* 34.

## APPENDIX 1. QUANTITATIVE SCANNING AUGER MICROSCOPY

It is possible to perform quantitative analysis using the scanning Auger microscope because the emission of the Auger electrons is proportional to the primary beam current ( $I_p$ ) and the primary beam energy ( $E_p$ )<sup>1</sup>. When these two variables are kept constant at levels that allow the microscope to analyze every electron produced (pulse counting), the following equation applies:

$$X_i = \frac{\frac{I_i}{S_i}}{\sum \frac{I_i}{S_i}} \quad (6.1)$$

Such that the atomic fraction of element  $i$  ( $X_i$ ) in the sample is equal to its corrected intensity ( $\frac{I_i}{S_i}$ ) divided by the sum of the corrected intensities of all of the elements in the sample. The corrected intensity is defined as the peak-to-peak intensity ( $I_i$ ) divided by the relative sensitivity ( $S_i$ ) for that element in an appropriate standard. In this experiment, the standard used was an  $Al_3Sc$  precipitate in a binary Al-0.5Sc alloy that had been aged to coarsen the precipitates. This was then compared with Auger spectra collected from a  $v$  precipitate in an ALS2 sample.

The first step in this calculation is to calculate the relative sensitivity of scandium ( $S_{Sc}$ ) in the non-lithium sample. We fix the value of  $S_{Al}$  to be unity and equation 6.1 becomes:

$$X_{Al} = \frac{I_{Al}}{I_{Al} + \frac{I_{Sc}}{S_{Sc}}} \quad (6.2)$$

Using values for  $I_{Al}$  and  $I_{Sc}$  from an  $Al_3Sc$  precipitate, the value of  $S_{Sc}$  can be directly calculated by fixing  $X_{Al}$  to be 0.75.

---

<sup>1</sup> Handbook of Auger Electron Spectroscopy, Perkin-Elmer Corporation, Eden Prairie, MI, 1978.



A spectrum is now taken from a sample  $\nu$  phase in ALS2 using the same values of  $I_p$  and  $E_p$ . Because this precipitate is assumed to contain lithium, the equation must now be modified to account for its presence.

$$X_{Al} = \frac{I_{Al}}{I_{Al} + \frac{I_{Sc}}{S_{Sc}} + \frac{I_{Li}}{S_{Li}}} \quad (6.3)$$

Using the value of  $S_{Sc}$  determined above and again fixing  $X_{Al}$  at 0.75, it is possible to calculate the value of  $\frac{I_{Li}}{S_{Li}}$ . Now, the atomic fraction of scandium in  $\nu$  phase can be

calculated from the equation:

$$X_{Sc} = \frac{I_{Sc}}{I_{Al} + \frac{I_{Sc}}{S_{Sc}} + \frac{I_{Li}}{S_{Li}}} \quad (6.4)$$

In performing these calculations the only assumptions being made are that the precipitates are all stoichiometric with respect to aluminum ( $X_{Al} = 0.75$ ) and that the value  $S_{Sc}$  remains constant for both samples.

## FIGURE CAPTIONS

- Figure 2.1. Phase diagram for the Al-Sc binary system (after Willey).
- Figure 2.2. Phase diagram for the Al-Li binary system (adapted from Flower).
- Figure 3.1. Diagram of the Light Alloy Melting Facility.
- Figure 3.2. Carbon filter design to improve degassing efficiency.
- Figure 3.3. Diagram of the copper chill blocks in the Light Alloy Melting Facility.
- Figure 3.4. Plot of cooling rate as a function of temperature for the top of a test ingot poured into the casting mold.
- Figure 3.5. Filter design used produce the ingots studied.
- Figure 3.6. Design of MgO crucible used in the Light Alloy Melting Facility.
- Figure 4.1. Diagram of rolling steps used on ALS2 for hot rolling and warm rolling.
- Figure 4.2. Diagram of rolling steps used for warm rolling of ALS4.
- Figure 4.3. Design of tensile samples used.
- Figure 5.1. Composite optical micrographs of as-cast ALS2 and ALS4 (Keller's etch, 30s ).
- Figure 5.2. Plot of three consecutive differential scanning calorimetry runs on a sample of as-cast ALS2.
- Figure 5.3. Bright field transmission electron micrograph of ALS2 (hot rolled, solution heat treated and peak aged) illustrating the grain boundary pinning of the  $Al_3Sc$  precipitates.
- Figure 5.4. Composite optical micrographs of rolled ALS2 and ALS4 (Keller's etch,30s).
- Figure 5.5. Optical micrographs of  $v$  phase in ALS4, as-cast and aged (top) and rolled and aged (bottom).
- Figure 5.6. Plot of DSC melting data for alloys with increasing lithium content.
- Figure 5.7. Optical micrographs of overaged ALS2 for phase equilibrium study (as-polished).
- Figure 5.8. Optical micrographs of overaged ALS4 for phase equilibrium study (as-polished).
- Figure 5.9. Scanning electron micrographs of overaged  $Al_3Sc$  precipitates in Al-0.5Sc-4Mg (sputter etched).

- Figure 5.10. Optical micrographs of ALS2 (450°C/ 48 hours) showing  $\nu$  phase and subgrains (sputter etched).
- Figure 5.11a. Comparison of ALS2 with other Al-Li-Zr alloys of varying lithium content.
- Figure 5.11b. Comparison of ALS4 with other Al-2.0Li-Mg-Zr alloys with varying magnesium content.
- Figure 5.12. Optical micrographs using Nomarski interference contrast of ALS2 (top) and ALS4 (bottom) deformed at 300 K to 6% plastic strain.
- Figure 5.13. Optical micrographs using Nomarski interference contrast of ALS2 (top) and ALS4 (bottom) deformed at 77 K to 15% plastic strain.
- Figure 5.14. Scanning electron micrograph of pre-polished ALS4 deformed at 300 K to 6% plastic strain.
- Figure 5.15. Scanning electron micrographs showing fracture surface of ALS2 tested at 300 K.
- Figure 5.16. Scanning electron micrographs showing fracture surface of ALS4 tested at 300 K.
- Figure 5.17. Scanning electron micrographs showing fracture surface of ALS2 tested at 77 K.
- Figure 5.18. Scanning electron micrographs showing fracture surface of ALS4 tested at 77 K.

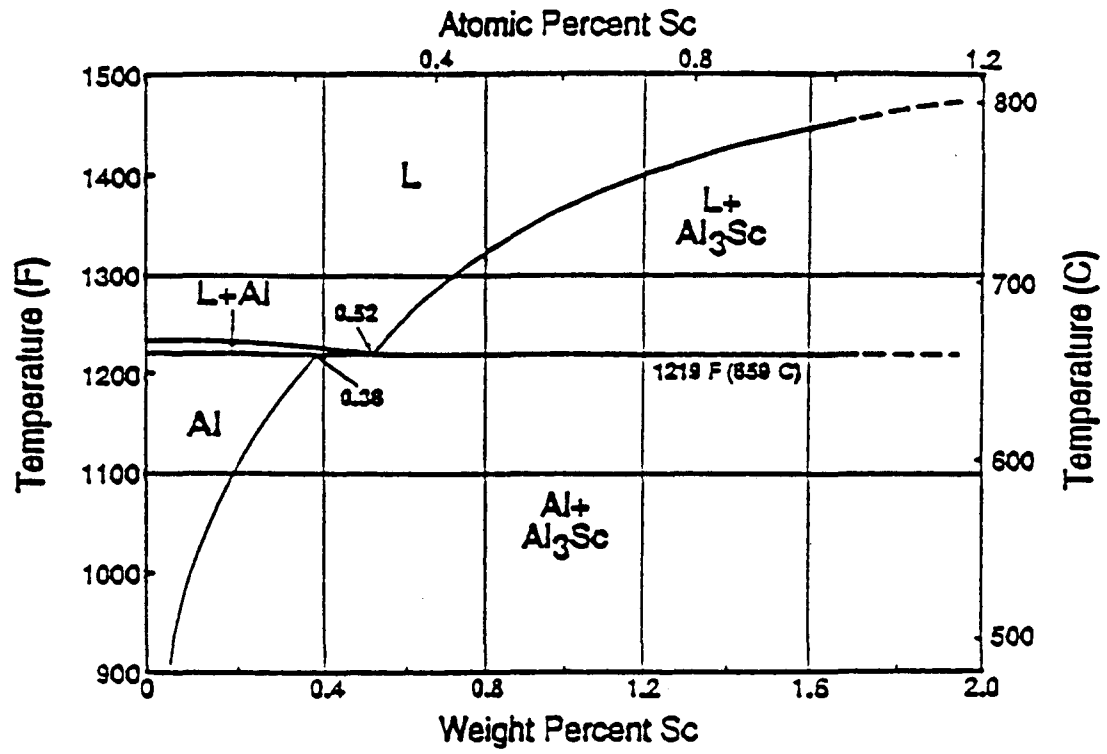


Figure 2.1. Phase diagram for the Al-Sc binary system (after Willey).

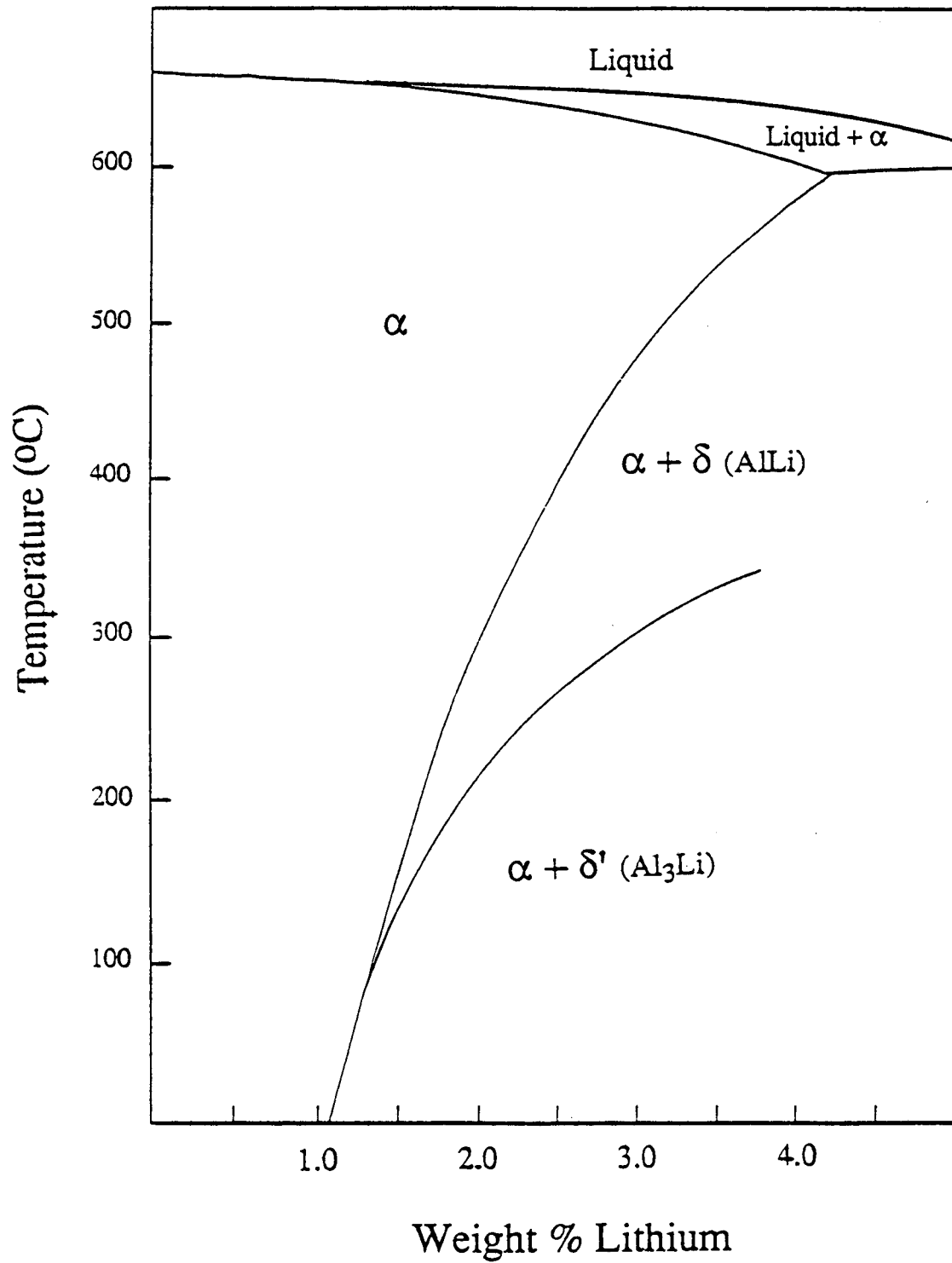


Figure 2.2. Phase diagram for the Al-Li binary system (adapted from Flower).

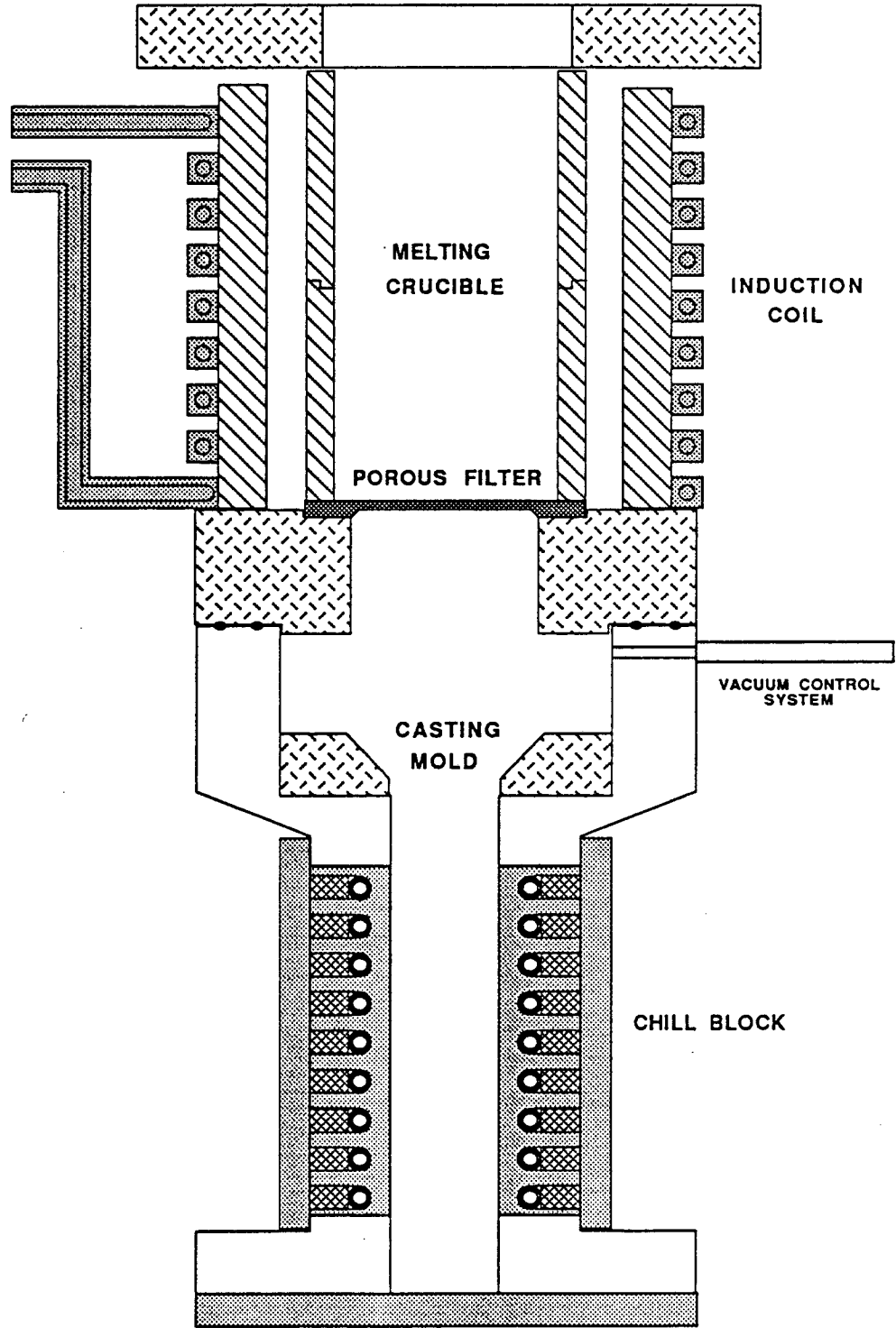


Figure 3.1. Diagram of the Light Alloy Melting Facility.

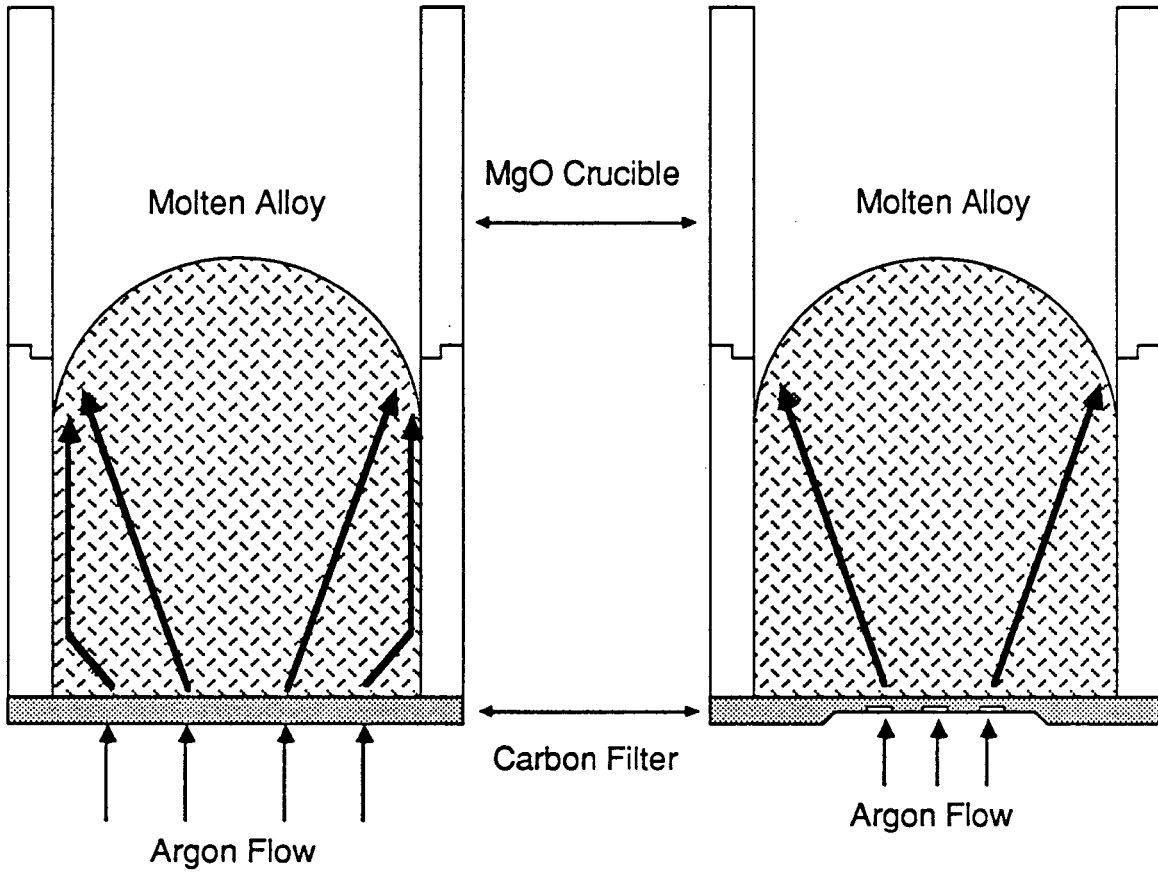


Figure 3.2. Carbon filter design to improve degassing efficiency.

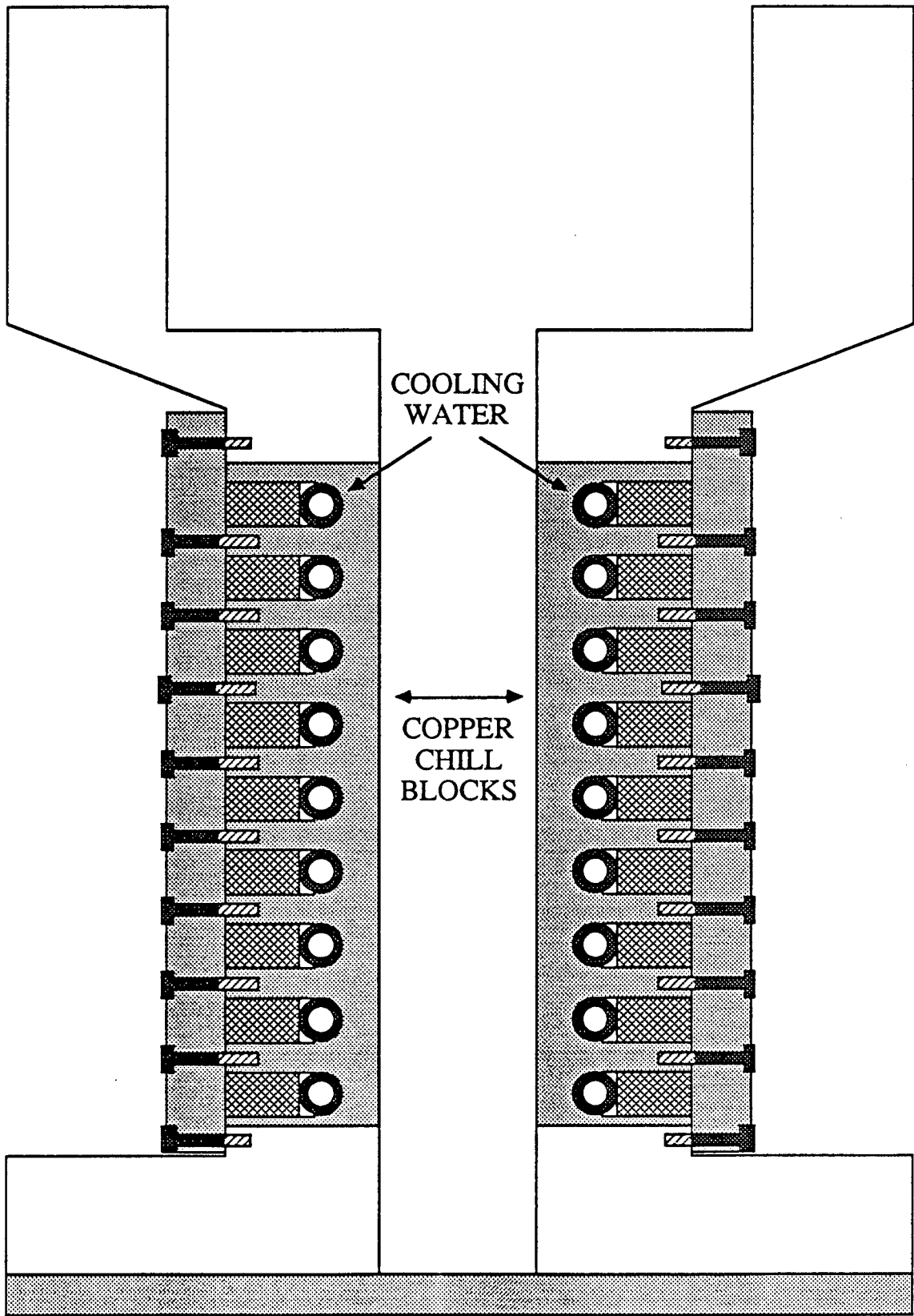


Figure 3.3. Diagram of the copper chill blocks in the Light Alloy Melting Facility.



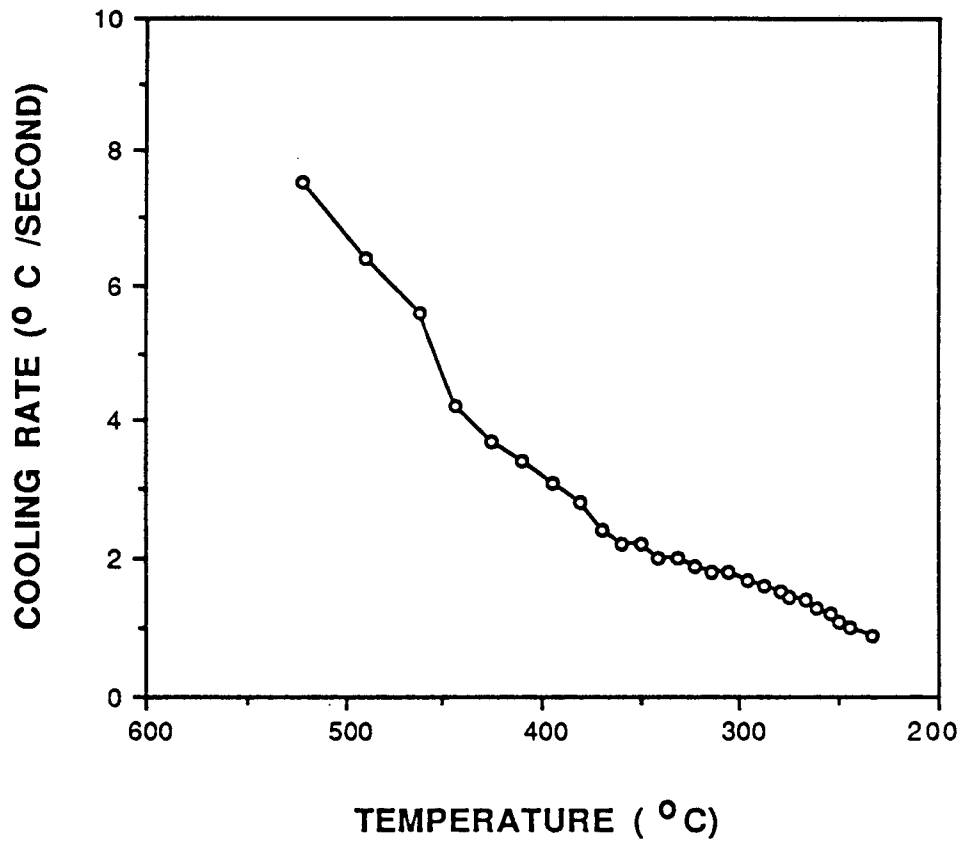


Figure 3.4. Plot of cooling rate as a function of temperature for the top of a test ingot poured into the casting mold.

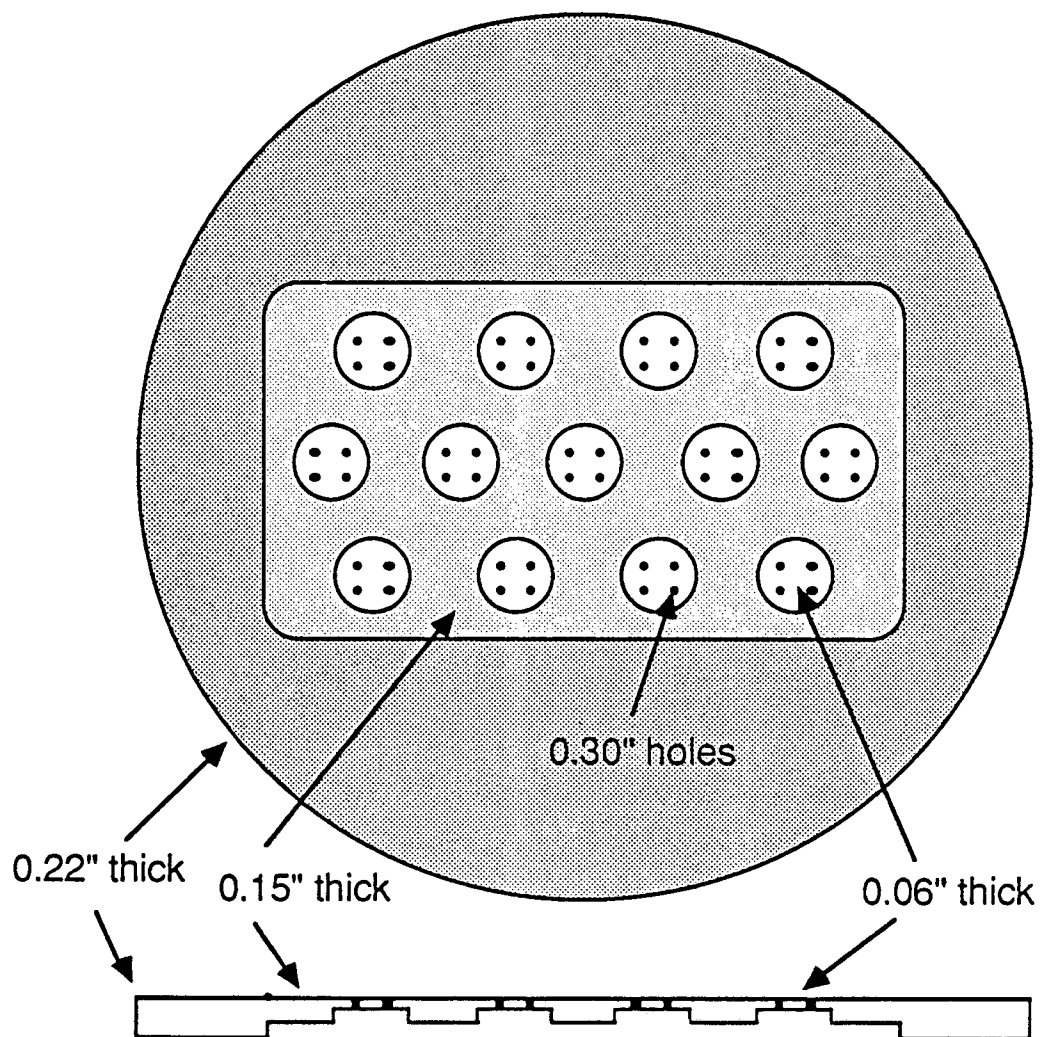


Figure 3.5. Design of graphite filter used to produce ingots studied.

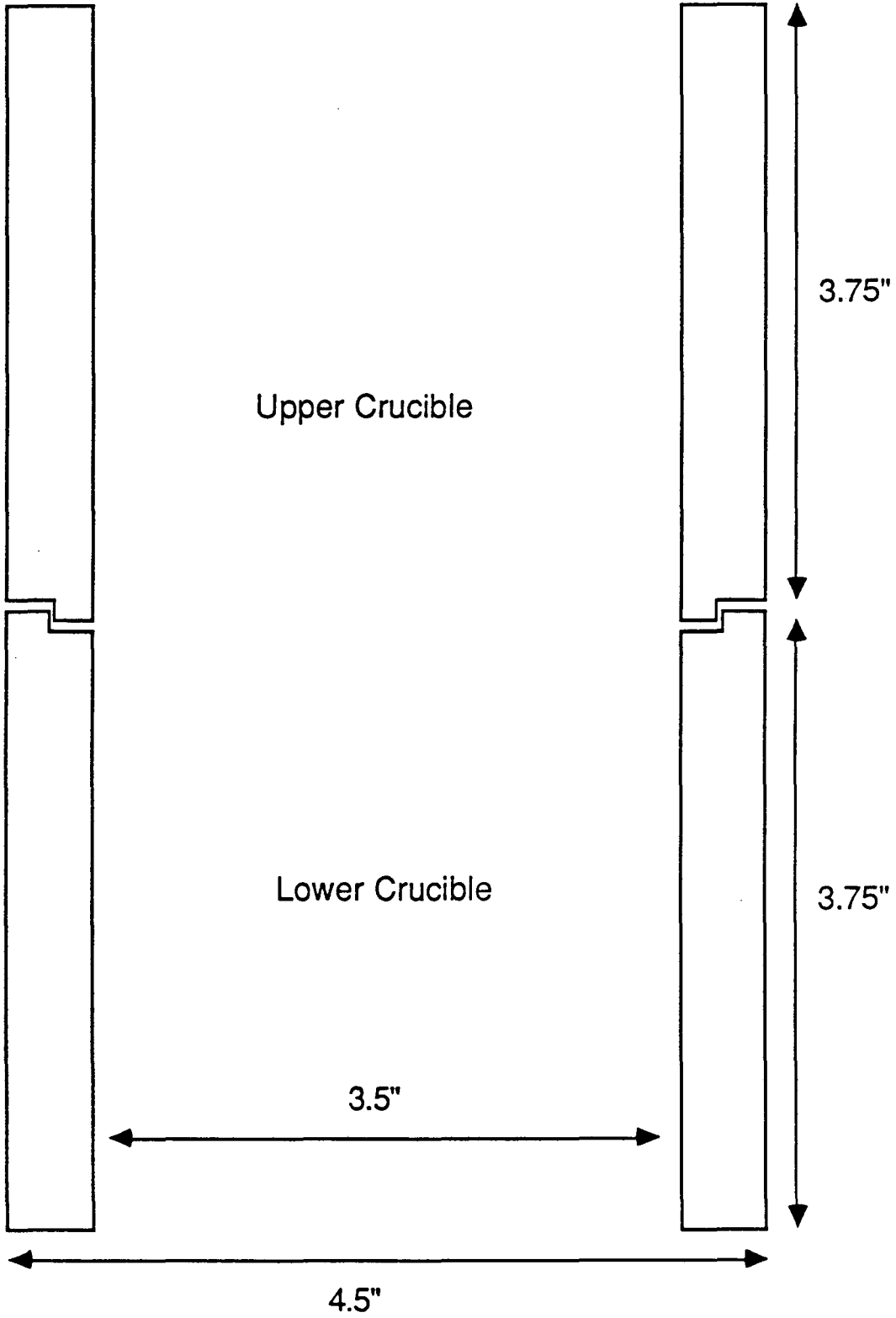


Figure 3.6. Design of MgO crucible used in the Light Alloy Melting Facility.

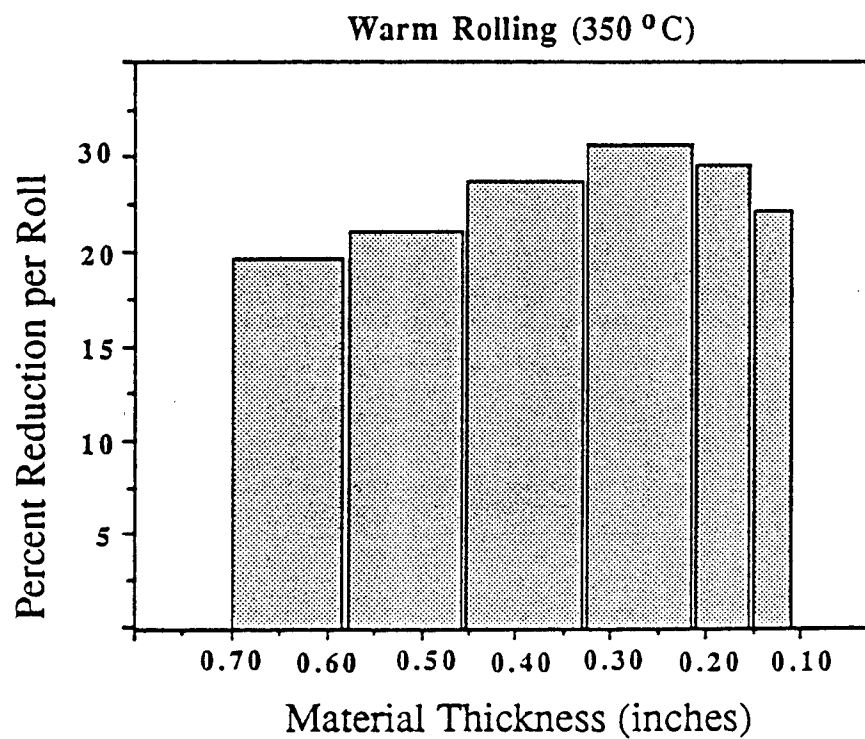
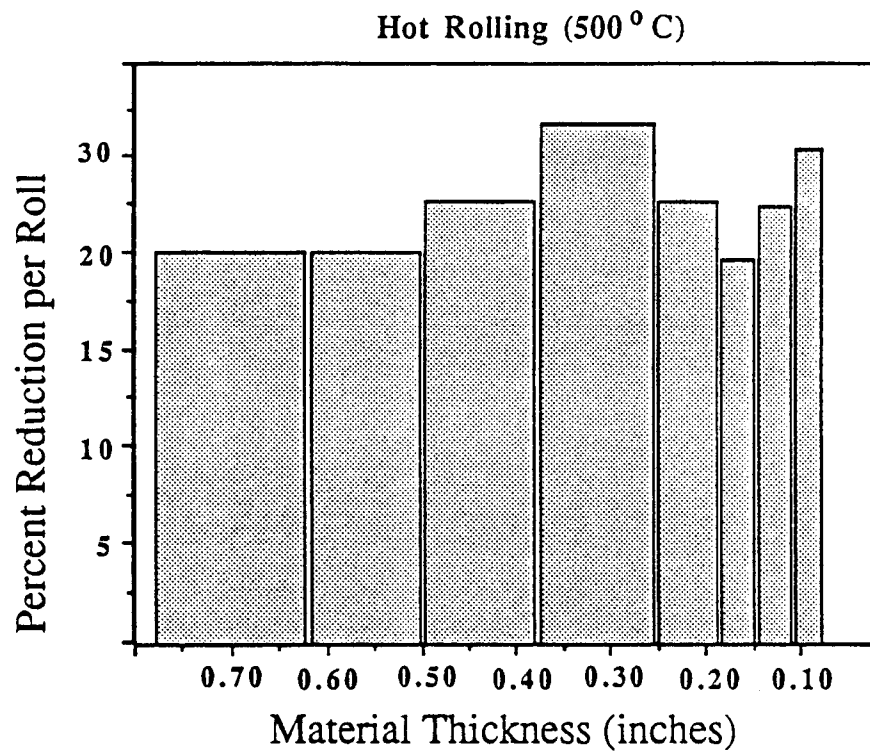


Figure 4.1. Diagram of rolling steps used on ALS2 for hot rolling and warm rolling.

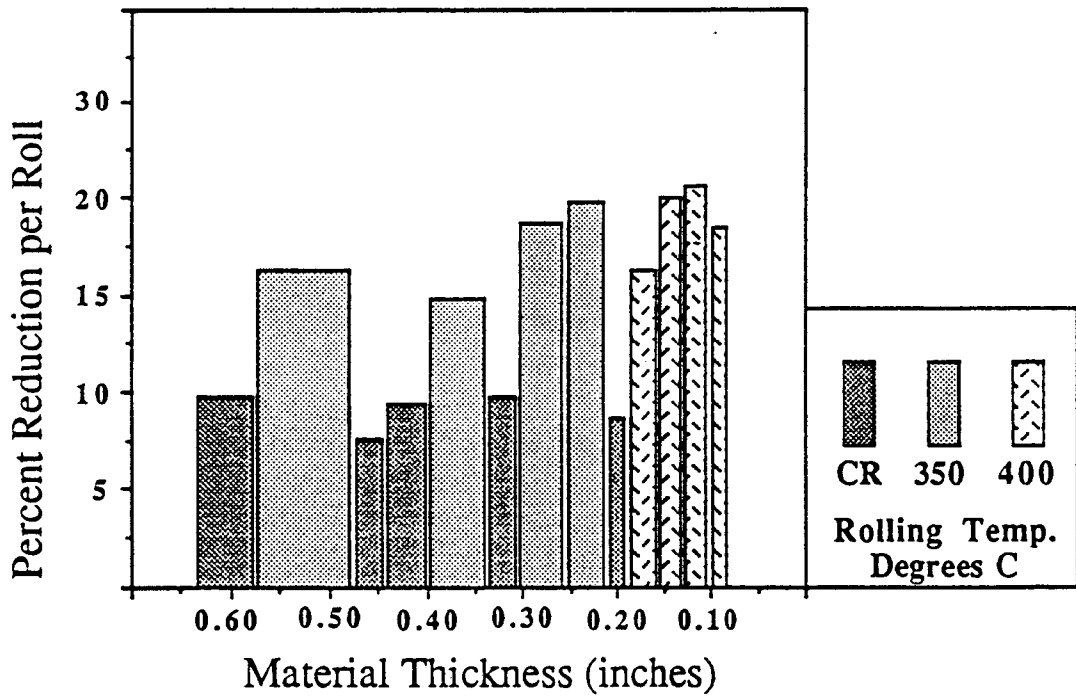


Figure 4.2. Diagram of rolling steps used for warm rolling of ALS4.

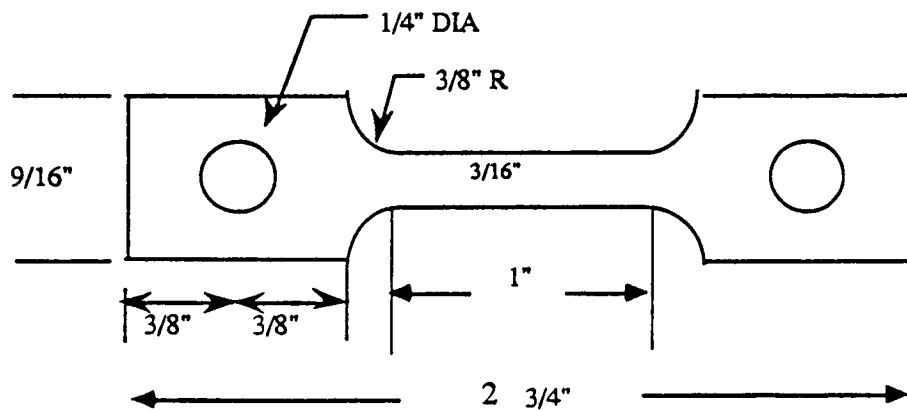


Figure 4.3. Design of tensile samples used.

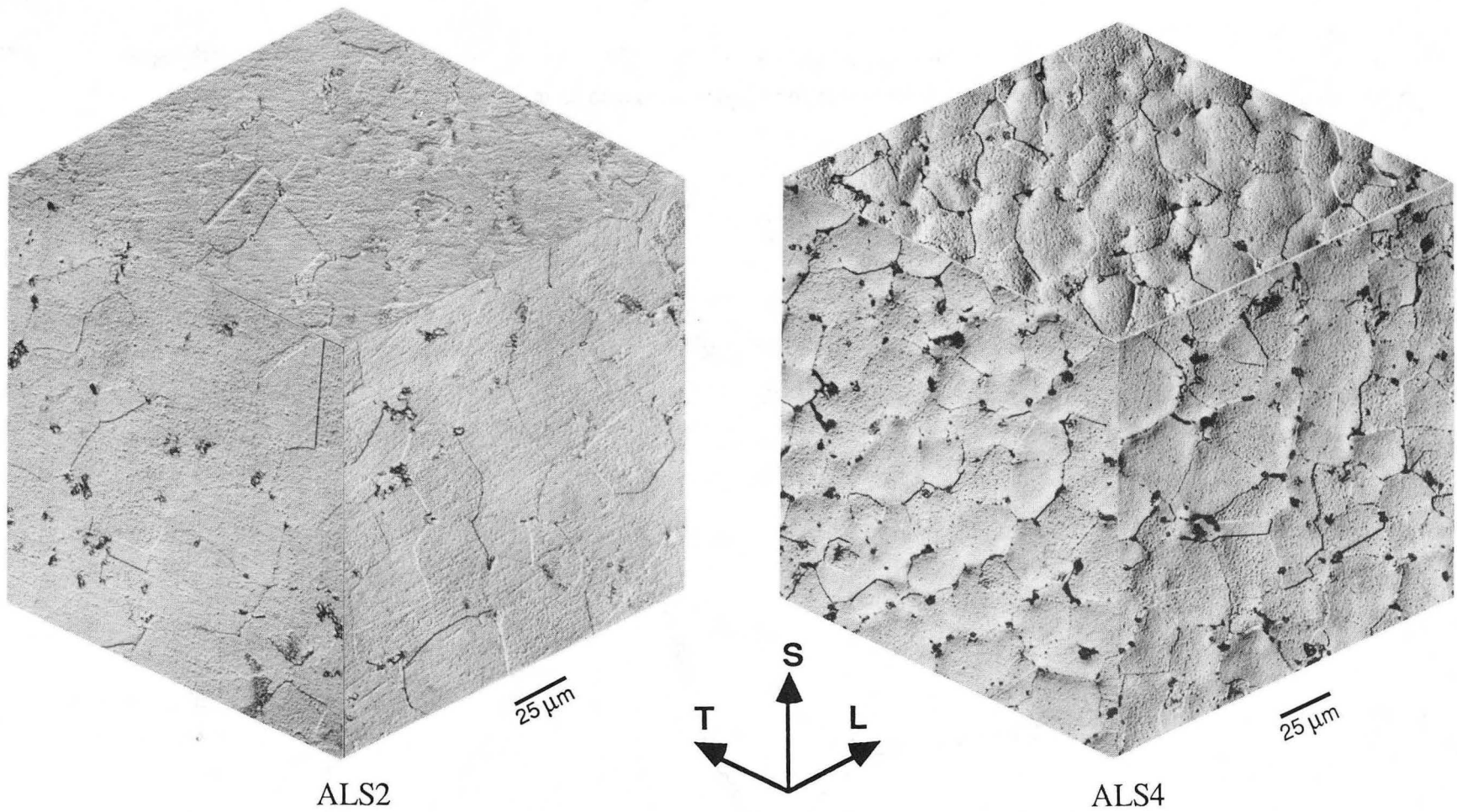


Figure 5.1. Composite optical micrographs of as-cast ALS2 and ALS4 (Keller's etch, 30s).

XBB 905-3549-A

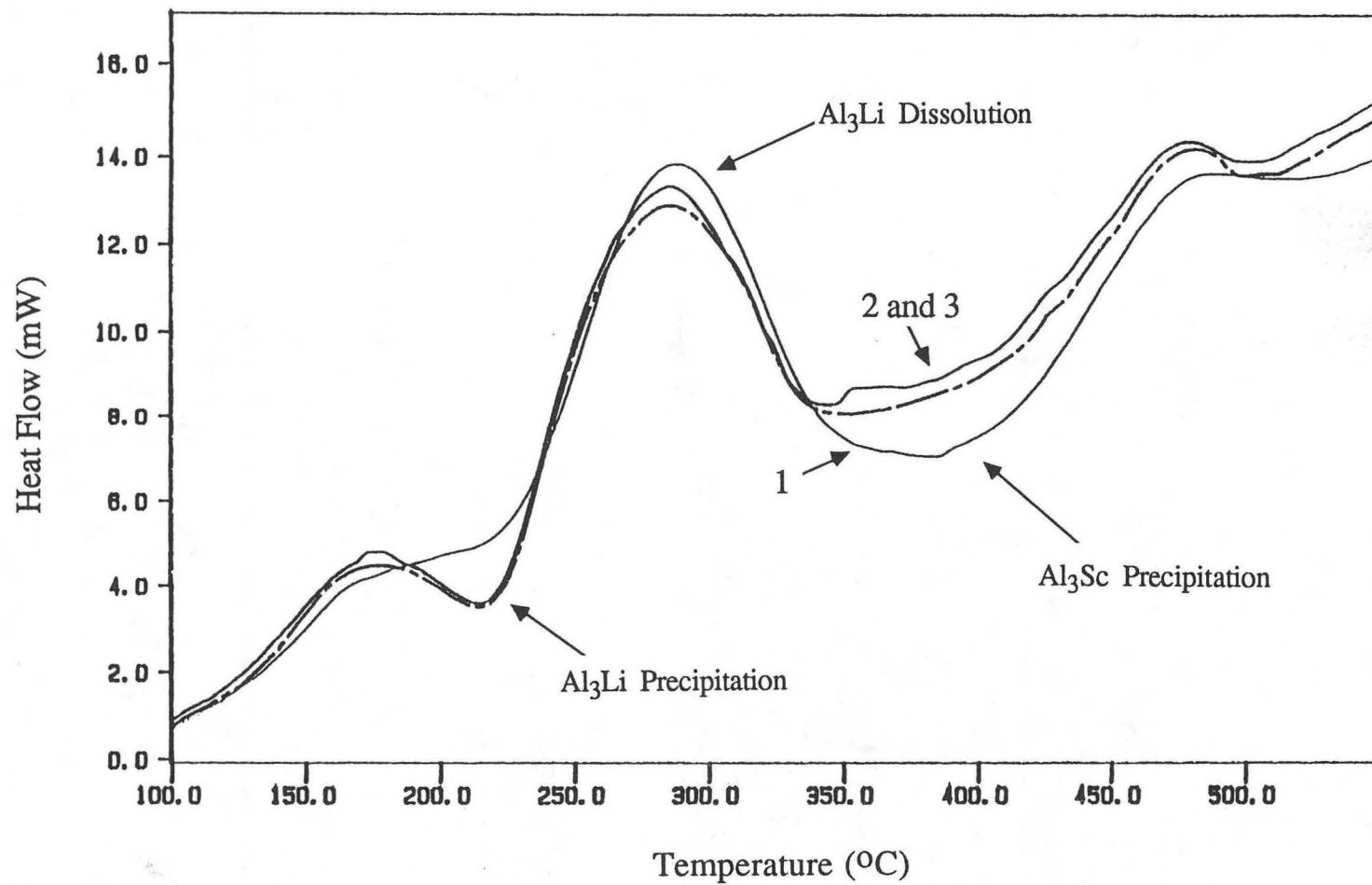
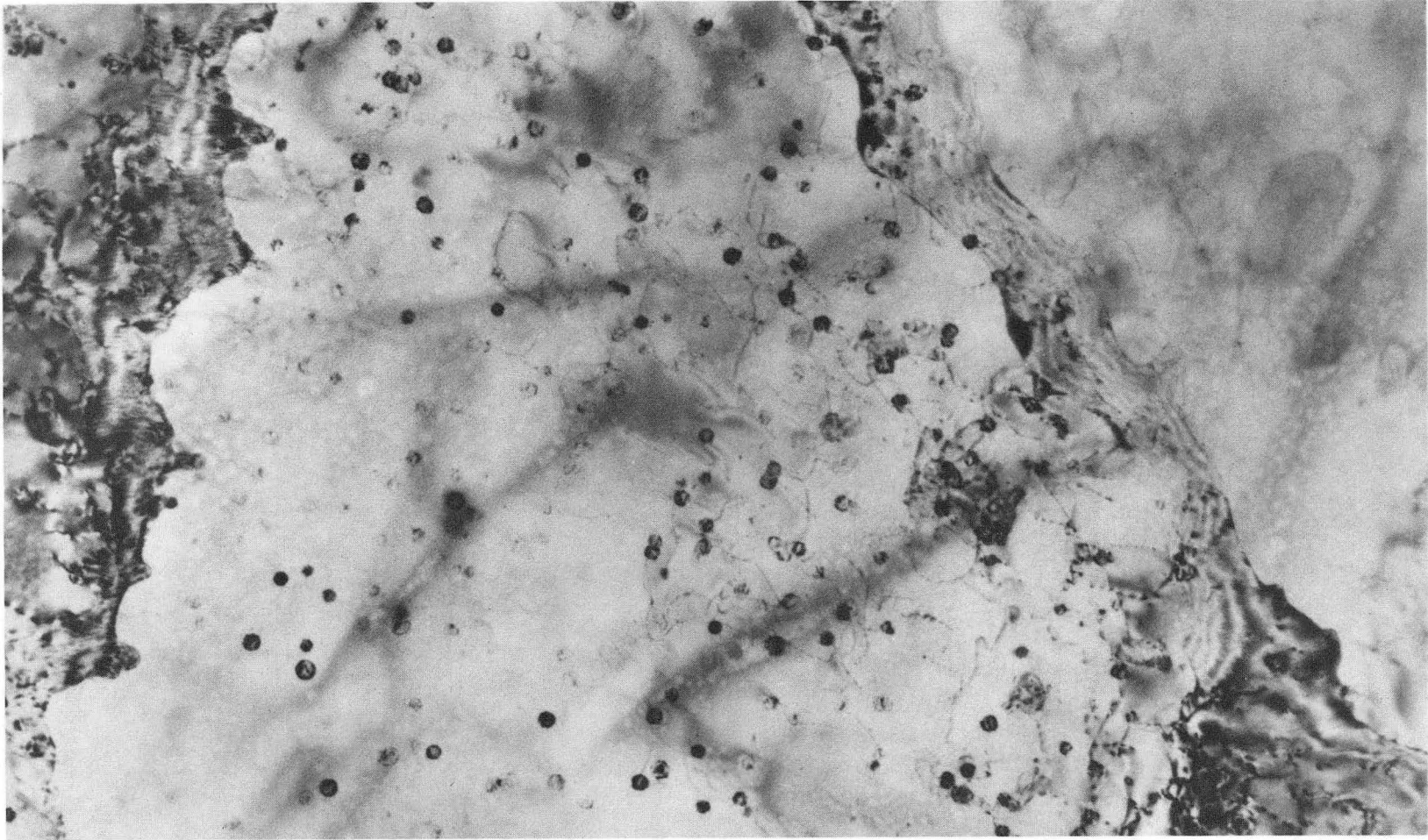


Figure 5.2. Plot of three consecutive differential scanning calorimetry runs on a sample of as-cast ALS2.



0.25  $\mu\text{m}$

Figure 5.3. Bright field transmission electron micrograph of ALS2 (hot rolled, solution heat treated and peak aged) illustrating the grain boundary pinning of the  $\text{Al}_3\text{Sc}$  precipitates.

XBB 906-5006



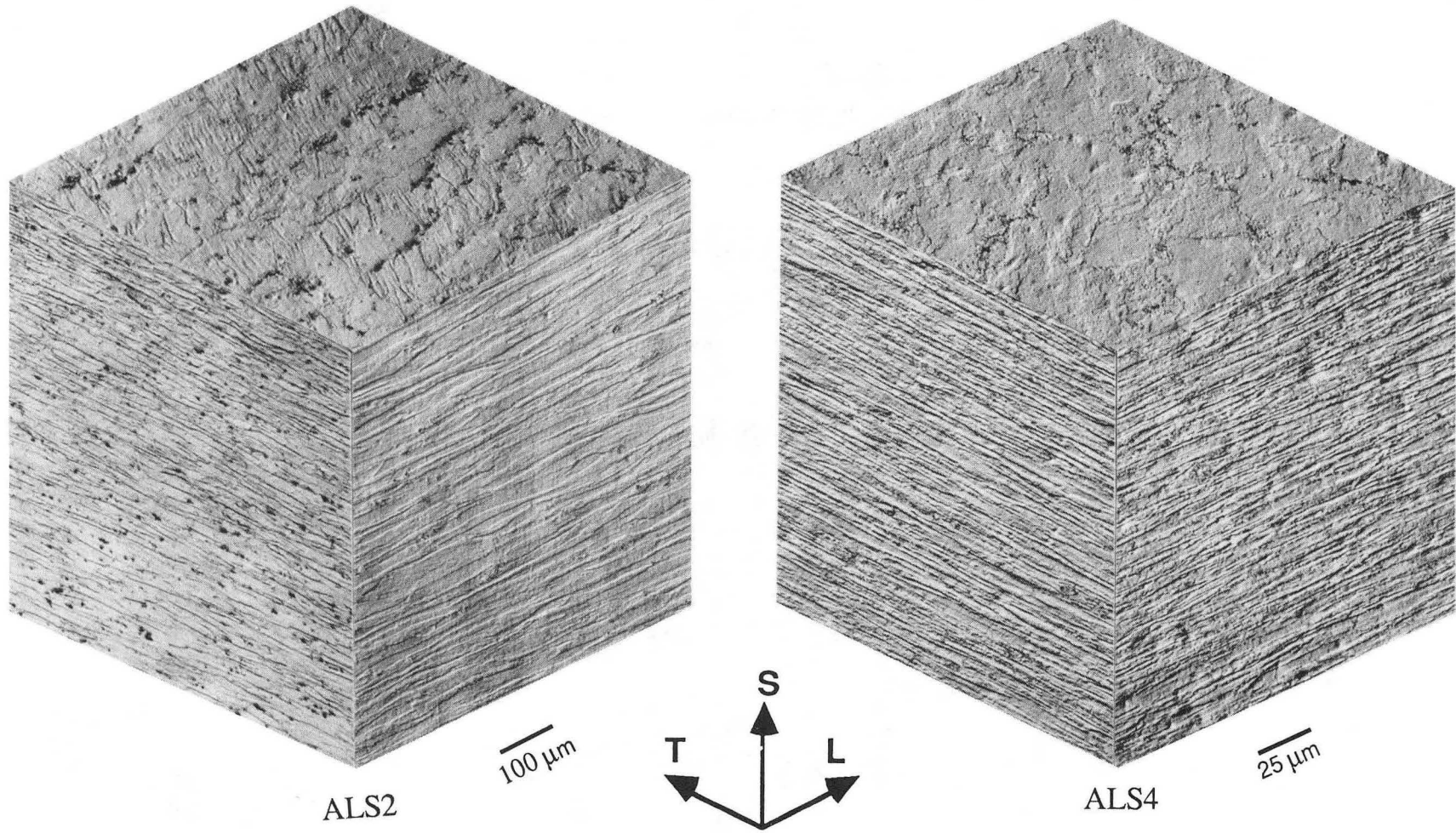


Figure 5.4. Composite optical micrographs of rolled ALS2 and ALS4 (Keller's etch, 30s).

XBB 905-3548-A



**As Cast + 350°C / 48 hours  
As Polished**

**20 μm**



**Rolled + 500°C / 24 hours  
As Polished**

**20 μm**

Figure 5.5. Optical micrographs of v phase in ALS4, as-cast and aged (top) and rolled and aged (bottom).

XBB 905-3552

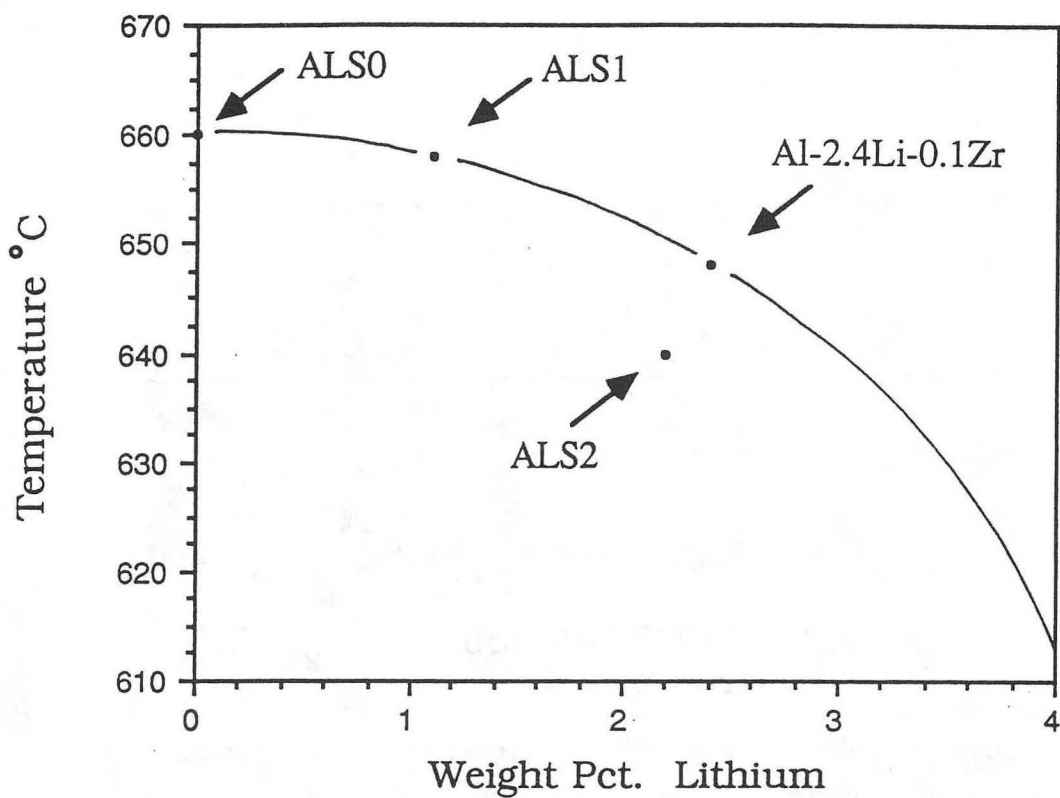
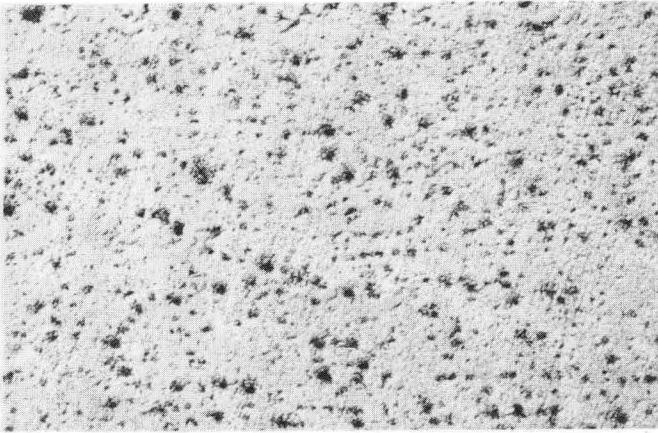


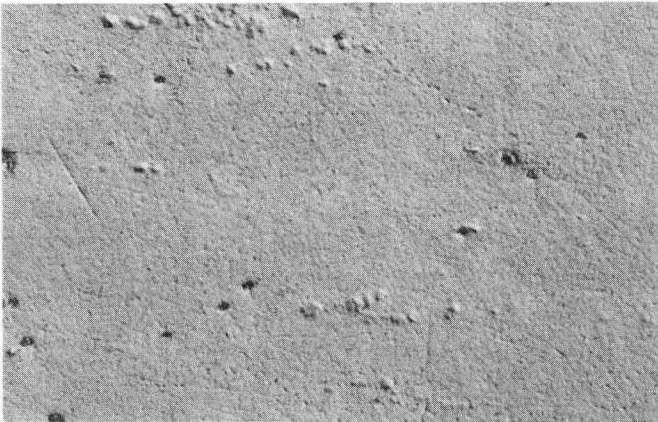
Figure 5.6. Plot of melting temperature (determined by differential scanning calorimetry) as a function of lithium content.



**A) 350°C/48 hours**



**B) 400°C / 48 hours**



**C) 450°C / 48 hours**



**D) 500°C / 24 hours** 50  $\mu\text{m}$

Figure 5.7. Optical micrographs of overaged ALS2 for phase equilibrium study (as-polished).

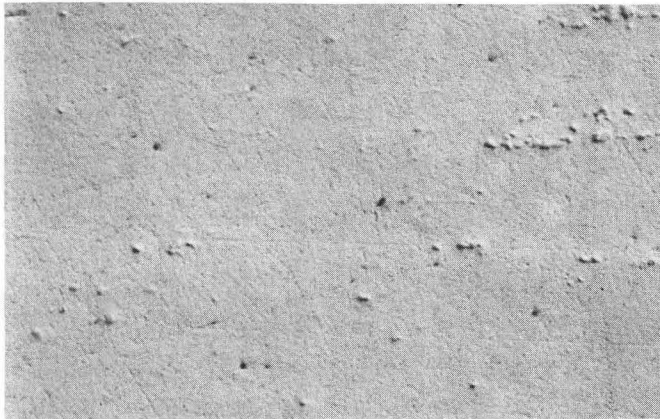
XBB 906-5004



**A) 350°C/48 hours**



**B) 400°C / 48 hours**



**C) 450°C / 48 hours**



**D) 500°C / 24 hours**

**50 μm**

Figure 5.8. Optical micrographs of overaged ALS4 for phase equilibrium study (as-polished).

XBB 906-5005

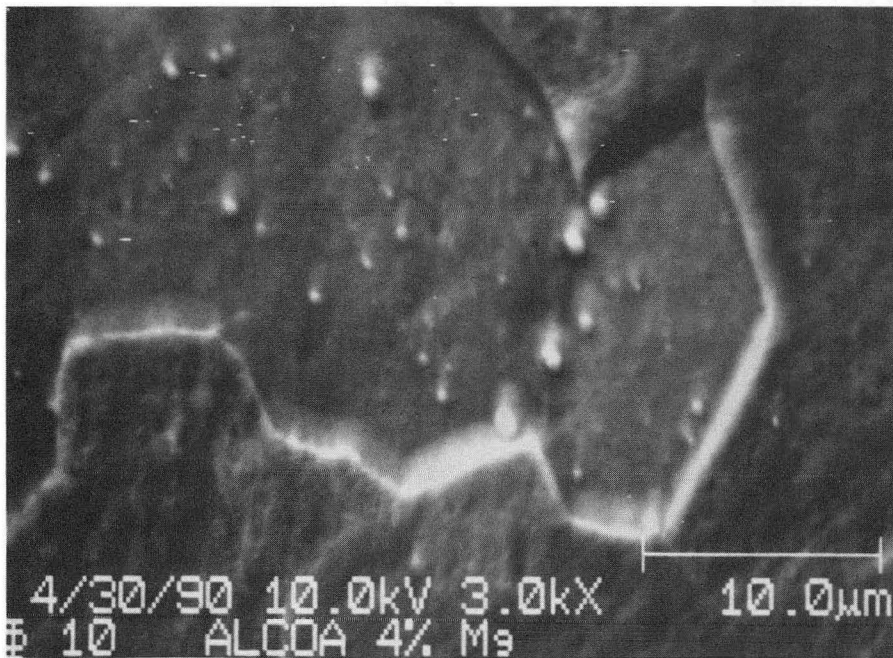
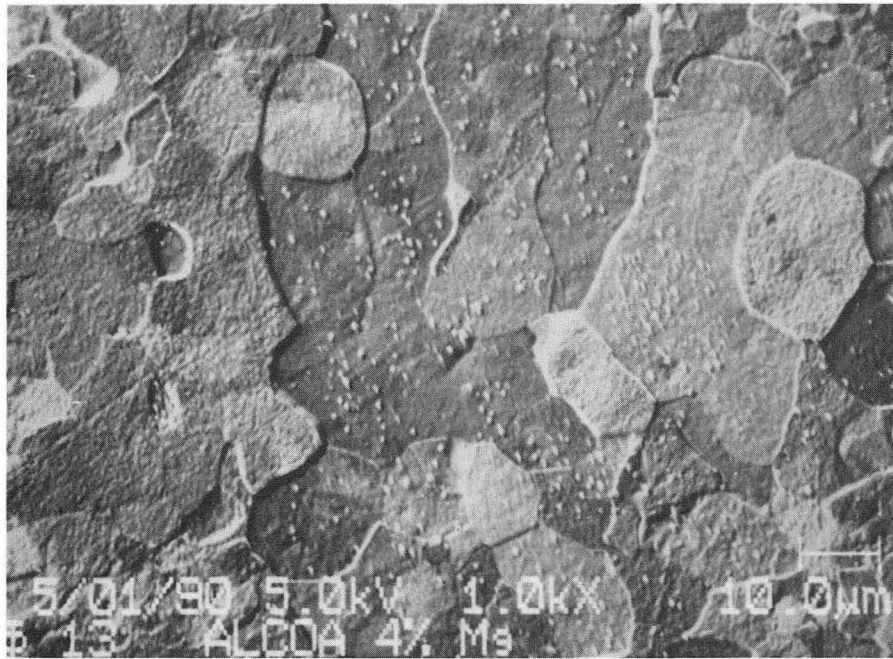


Figure 5.9. Scanning electron micrographs of overaged  $\text{Al}_3\text{Sc}$  precipitates in  $\text{Al-0.5Sc-4Mg}$  (sputter etched).

XBB 905-3542



20  $\mu\text{m}$



20  $\mu\text{m}$

XBB 905-3550

Figure 5.10. Optical micrographs of ALS2 (450°C/ 48 hours) showing v phase and subgrains (sputter etched).

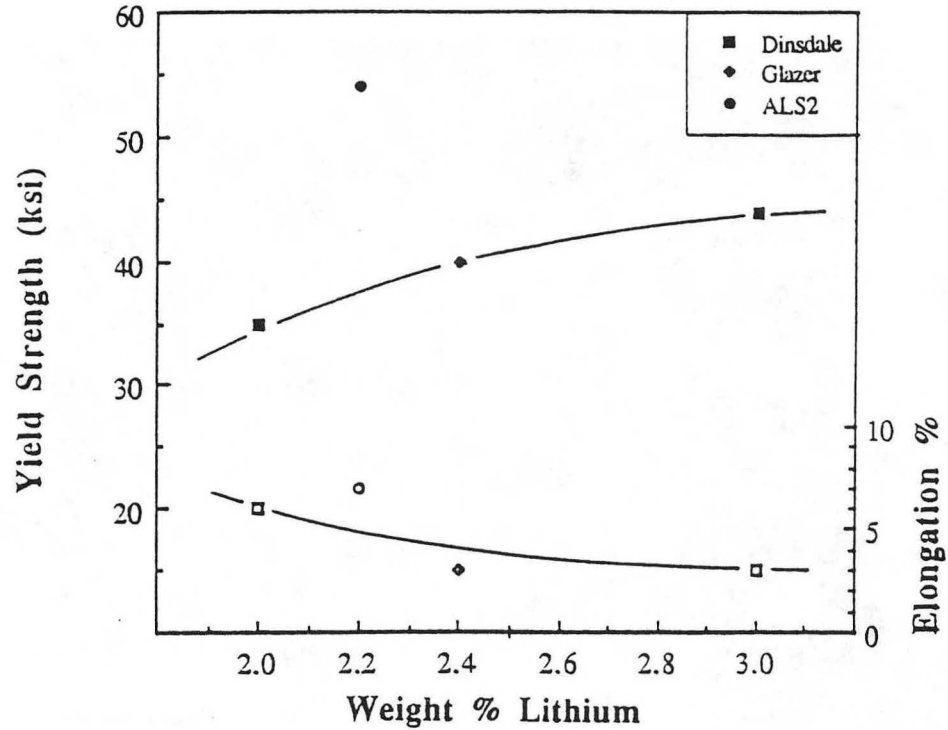


Figure 5.11a. Comparison of ALS2 with other Al-Li-Zr alloys of varying lithium content.

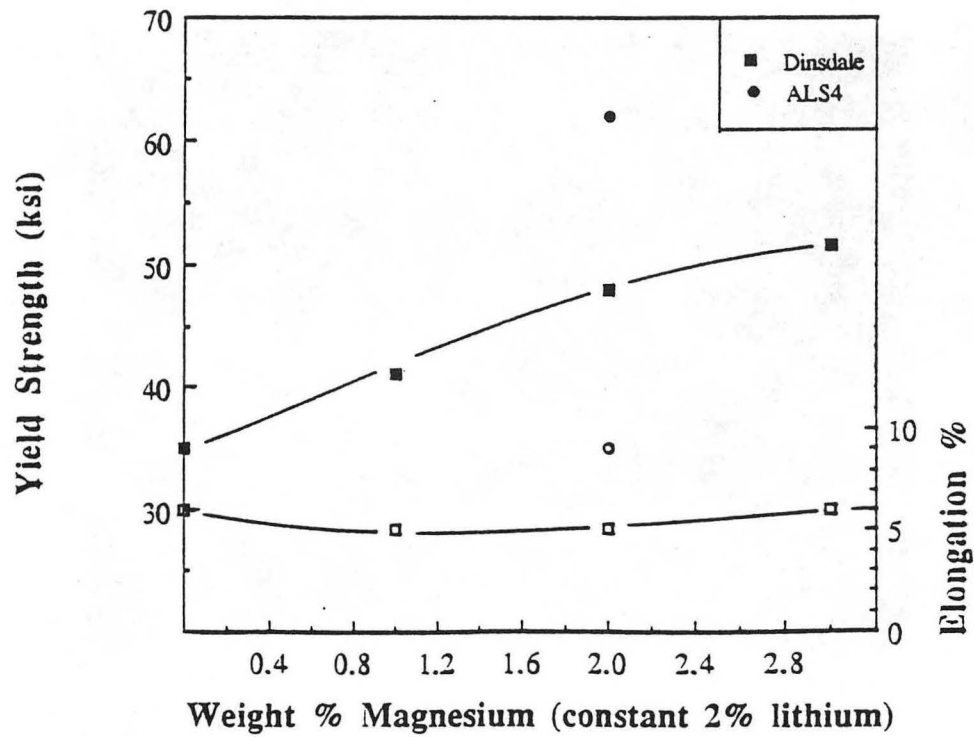
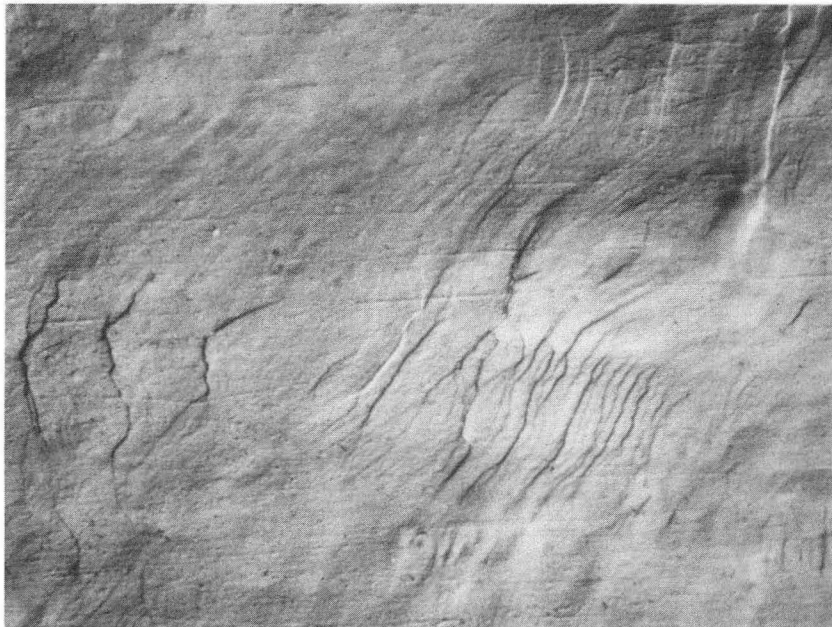


Figure 5.11b. Comparison of ALS4 with other Al-2.0Li-Mg-Zr alloys with varying magnesium content.



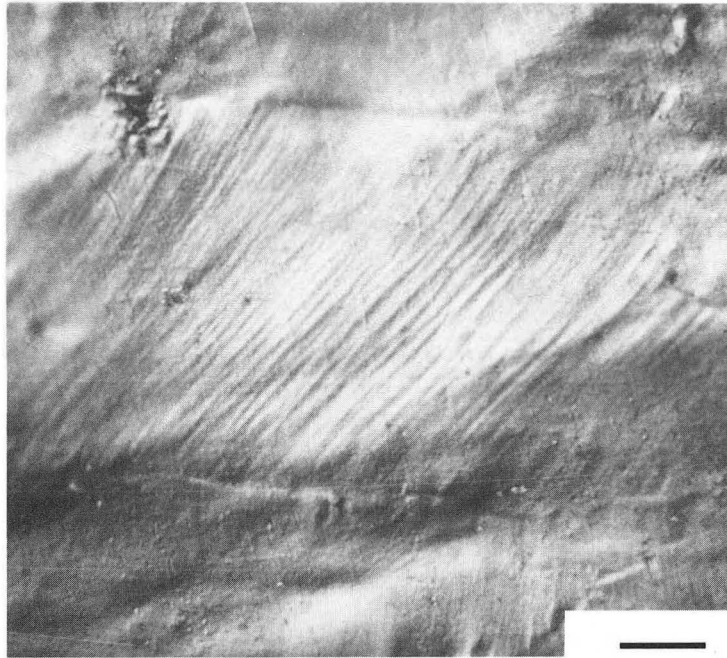


20  $\mu\text{m}$

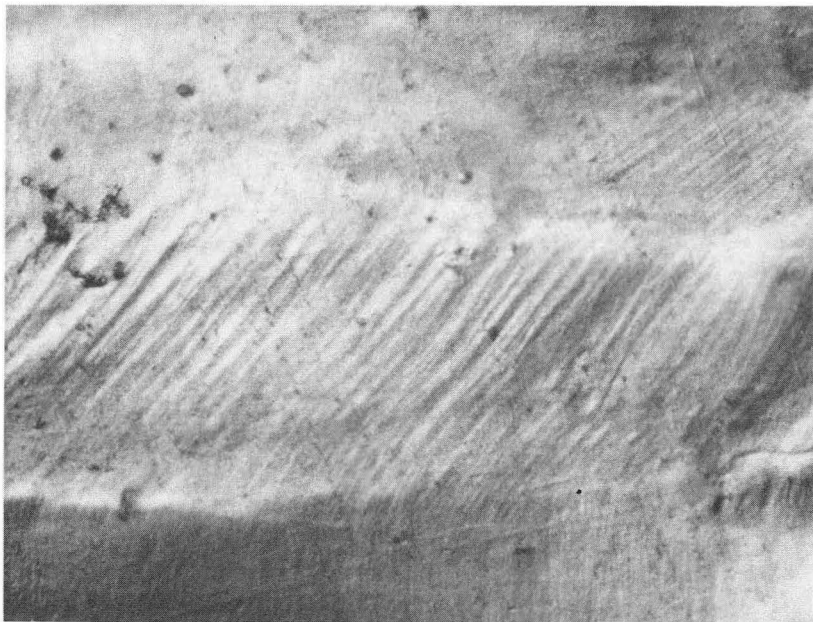


20  $\mu\text{m}$

Figure 5.12. Optical micrographs using Nomarski interference contrast of ALS2 (top) and ALS4 (bottom) deformed at 300 K to 6% plastic strain.



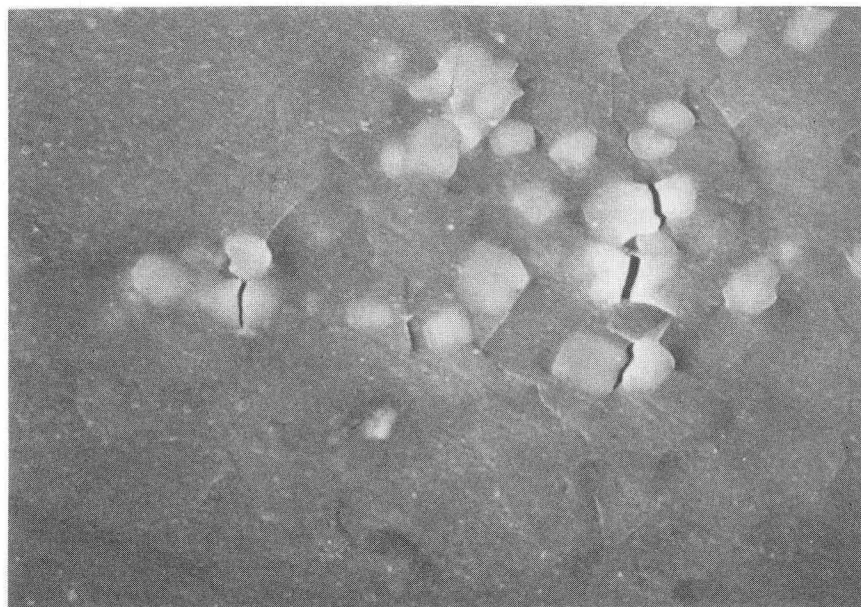
10  $\mu\text{m}$



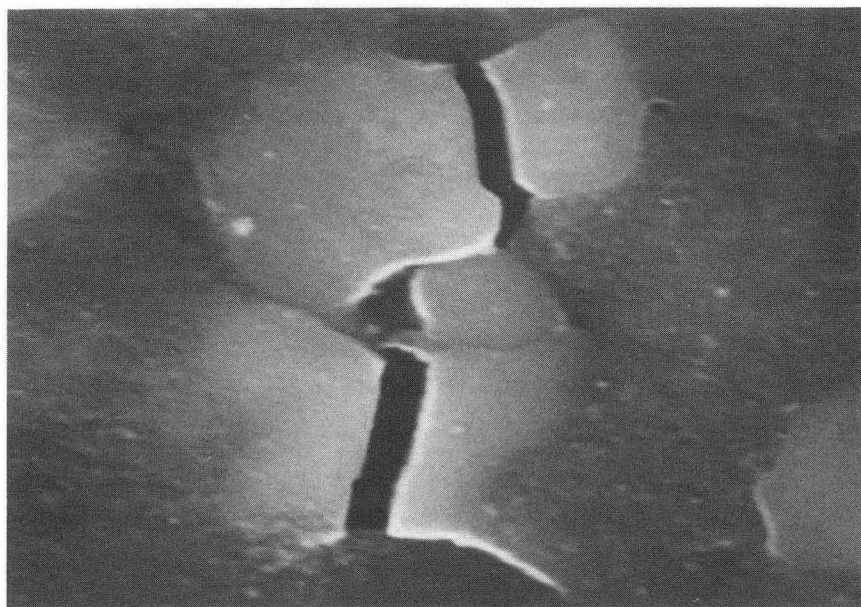
10  $\mu\text{m}$

XBB 906-5080

Figure 5.13. Optical micrographs using Nomarski interference contrast of ALS2 (top) and ALS4 (bottom) deformed at 77 K to 15% plastic strain.



8.0  $\mu\text{m}$

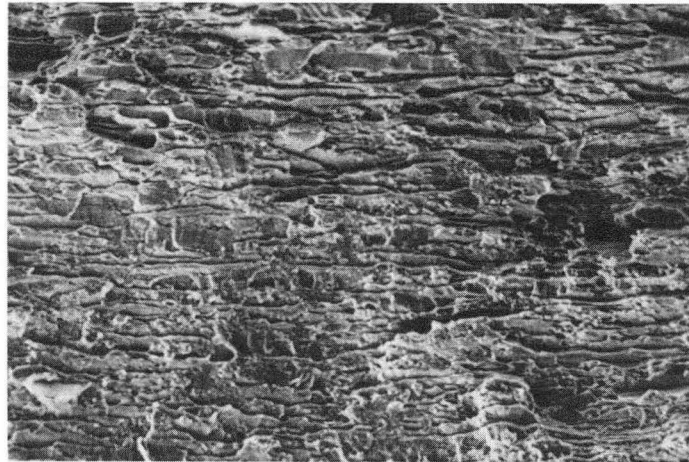


2.0  $\mu\text{m}$

XBB 906-4562

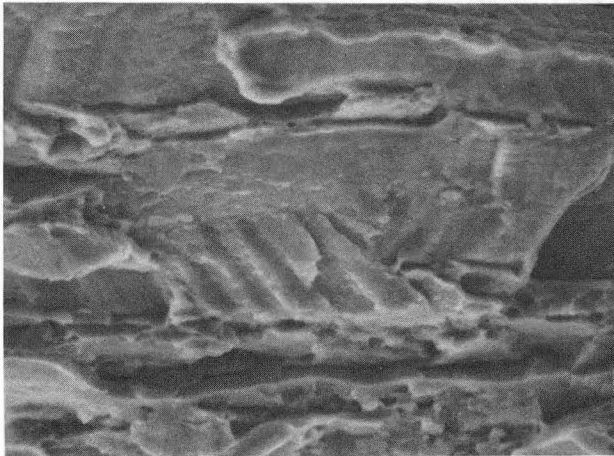
Figure 5.14. Scanning electron micrograph of pre-polished ALS4 deformed at 300 K to 6% plastic strain.

$\epsilon_{\text{plastic}} = 6\%$   
 $\sigma_{\text{true}} = 65 \text{ ksi}$

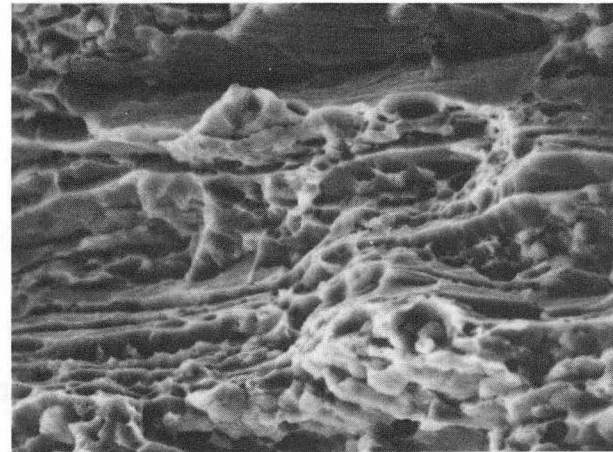


100  $\mu\text{m}$

XBB 906-4565



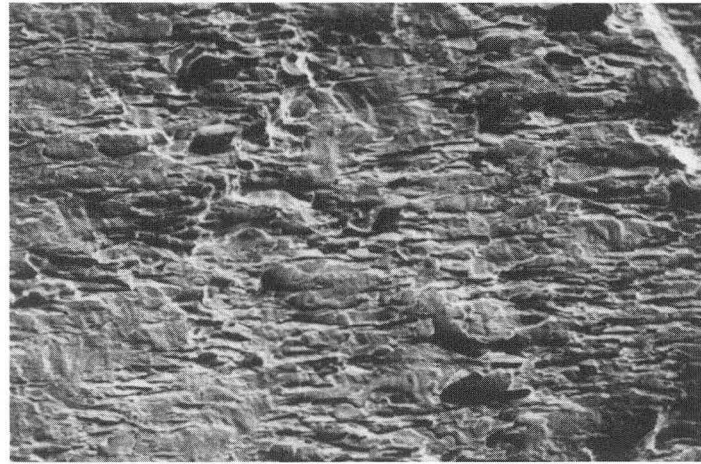
20  $\mu\text{m}$



20  $\mu\text{m}$

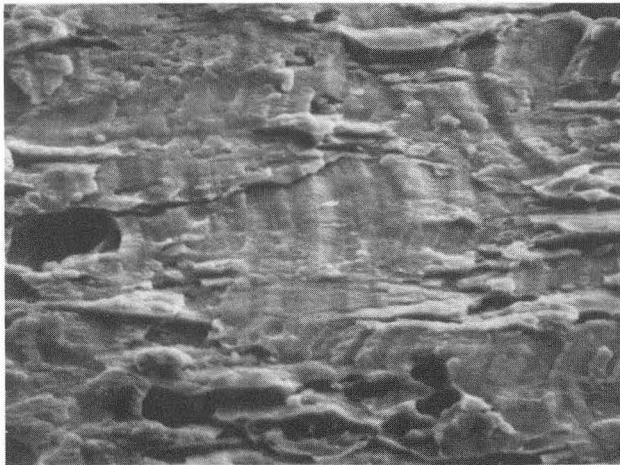
Figure 5.15. Scanning electron micrographs showing fracture surface of ALS2 tested at 300 K.

$\epsilon_{\text{plastic}} = 9\%$   
 $\sigma_{\text{true}} = 76 \text{ ksi}$

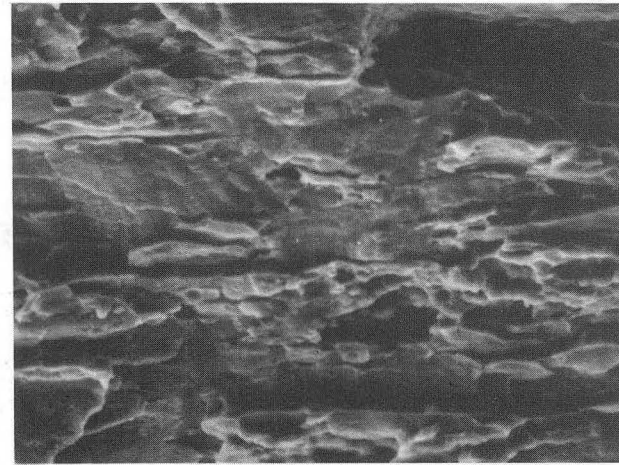


100  $\mu\text{m}$

XBB 906-4563



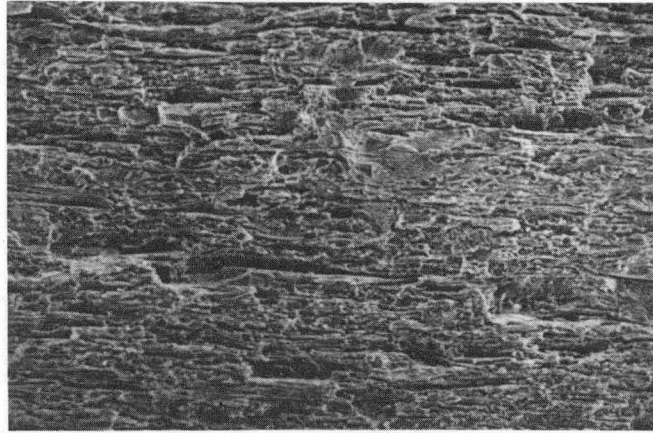
20  $\mu\text{m}$



20  $\mu\text{m}$

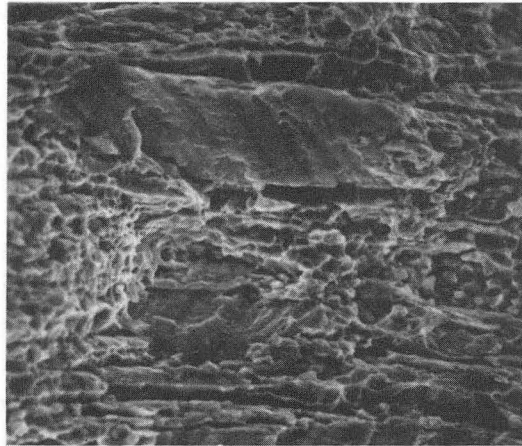
Figure 5.16. Scanning electron micrographs showing fracture surface of ALS4 tested at 300 K.

$\epsilon_{\text{plastic}} = 14\%$   
 $\sigma_{\text{true}} = 90 \text{ ksi}$

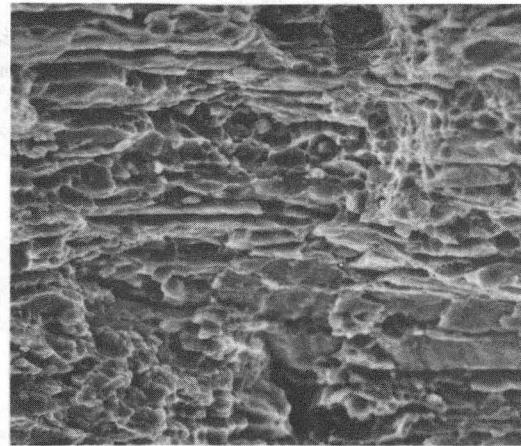


100  $\mu\text{m}$

XBB 906-4566



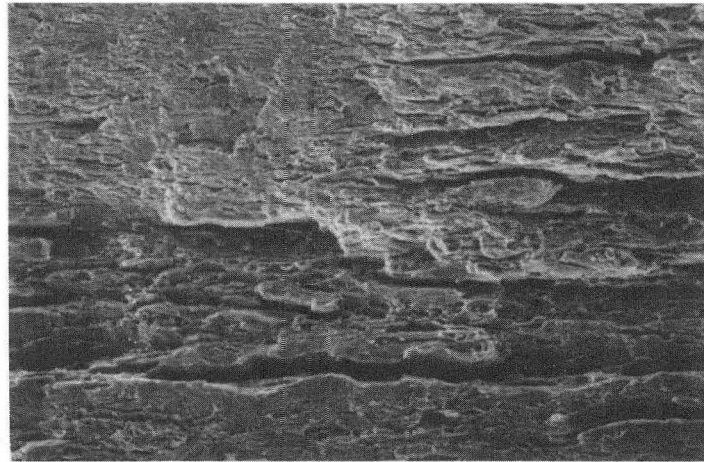
20  $\mu\text{m}$



20  $\mu\text{m}$

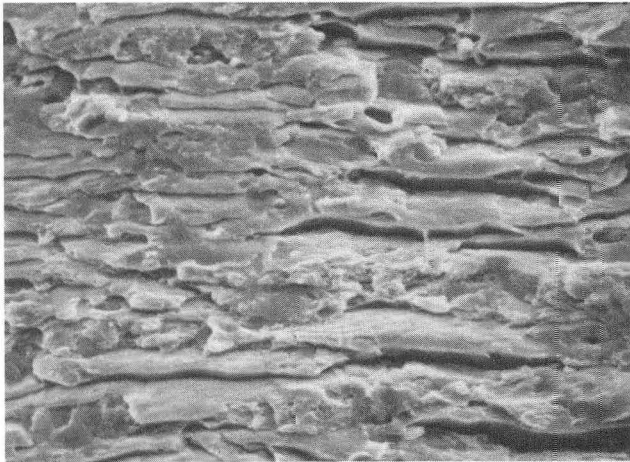
Figure 5.17. Scanning electron micrographs showing fracture surface of ALS2 tested at 77 K.

$\epsilon_{\text{plastic}} = 21\%$   
 $\sigma_{\text{true}} = 105 \text{ ksi}$

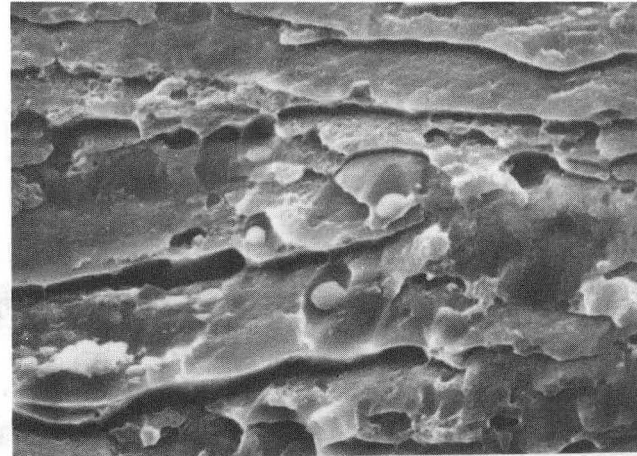


100  $\mu\text{m}$

XBB 906-4564



20  $\mu\text{m}$



5.0  $\mu\text{m}$

Figure 5.18. Scanning electron micrographs showing fracture surface of ALS4 tested at 77 K.

LAWRENCE BERKELEY LABORATORY  
CENTER FOR ADVANCED MATERIALS  
1 CYCLOTRON ROAD  
BERKELEY, CALIFORNIA 94720